R66-21

SECONDARY MOTION AND TURBULENCE IN CIRCULAR COUETTE FLOW

by
L. W. Gelhar
W. Schriek
F. A. Benham

HYDRODYNAMICS LABORATORY
REPORT NO. 97

Prepared Under
Research Grant No. GK-110
Engineering Division
National Science Foundation

Ju[illegible] 66

MIT

DEPARTMENT OF CIVIL ENGINEERING

SCHOOL OF ENGINEERING
MASSACHUSETTS INSTITUTE OF TECHNOLOGY
Cambridge 39, Massachusetts

R66-21

HYDRODYNAMICS LABORATORY
Department of Civil Engineering
Massachusetts Institute of Technology

SECONDARY MOTION AND TURBULENCE IN CIRCULAR COUETTE FLOW

by

L. W. Gelhar, W. Schriek, and F. A. Benham

July, 1966

Report No. 97

Prepared Under
Research Grant No. GK-110
Engineering Division
National Science Foundation

ABSTRACT

The flow in an annular space between two separately rotating cylinders of finite length is investigated. It is found that when the outer cylinder rotates faster than, and in the same direction as, the inner cylinder, the fluid moves largely in solid body rotation with the outer cylinder. In order to understand the dynamics of this type of flow, a laminar theory is formulated. The equations of motion are linearized by developing the solution as a perturbation of the state of solid body rotation. The theory predicts tangential velocities which are independent of the axial co-ordinate in the interior region. It also predicts the streamline pattern of the secondary motion in that region.

The observed tangential velocities at mid-height in the annular space, using water and air, are in good agreement with the predicted velocities from the theory. Hot wire anemometers are used for the measurement of turbulence intensities in air. In light of these measurements the agreement with the theory is somewhat surprising, since the flow is observed to be turbulent in all the experiments. The turbulence intensities near the inner cylinder wall are found to be of the same order of magnitude as those found near the wall in pipe flow.

ACKNOWLEDGEMENTS

The work reported herein is part of an experimental and analytical study of hydraulic and sedimentary processes in the annular space between two concentric rotating cylinders which is sponsored by the National Science Foundation under Grant No. GK-110. The M.I.T. Division of Sponsored Research has administered the grant under the project designation DSR 4527.

The work was carried out in the Hydrodynamics Laboratory of the Department of Civil Engineering at the Massachusetts Institute of Technology by Willem Schriek and Frank A. Benham, Research Assistants in Civil Engineering, under the supervision of Dr. Arthur T. Ippen, Ford Professor of Engineering, and Dr. Lynn W. Gelhar, Assistant Professor of Civil Engineering.

The computational services of the M.I.T. Civil Engineering Systems Laboratory were employed in this study.

TABLE OF CONTENTS

LIST OF FIGURES

CHAPTER I

INTRODUCTION

In the past, engineers and researchers have devoted considerable time and energy to the study of sediment transport. Analyses of data collected from rivers and canals, which transport sedimentary material over a bed or in suspension or both, have been used in the development of empirical formulas to predict rates of erosion and deposition. The formulas are empirical in that they represent the alternatives which most closely fit the observations, but lack the support of a rational basis.

In an attempt to approach this problem on a more rational basis, researchers have used rectangular flumes with adjustable slopes and cross-sections, in which alignment as well as water and sediment discharges were accurately controlled.

To further increase control over flow conditions a special experimental facility was conceived for the study of sedimentary processes. This apparatus consists of two concentric cylinders both of which rotate separately about a vertical axis, creating a rectangular annular space. The annular space is closed at both ends so that it can contain a mixture of water and sediments. At moderate rates of rotation of the cylinders the centrifugal acceleration will force the denser particles to form a layer on the outer cylinder wall which is analogous to the bed of an open channel. By introducing a differential rotation between the cylinders, a shear is introduced which, when sufficiently large, will cause erosion of the particles from the layer at the outer cylinder wall. The annular space is thus in effect an infinitely long rectangular channel in which possible disturbances due

to entrance and exit conditions have been eliminated. Measurement of the total shear force on a cylinder surface allows the determination of the energy gradient. This is equivalent to the slope measurement of a uniform flow in a rectangular channel.

The flow of homogeneous fluids between concentric rotating cylinders has been subject to extensive experimental and theoretical study. As early as 1916, Lord Rayleigh (1) noted that an inviscid fluid flow between two concentric cylinders rotating in the same direction, is stable with respect to axisymmetric disturbances when the circulation increases continuously with the radius. Taylor (2) extended the analysis when he investigated the stability of viscous liquid flow between rotating cylinders with a low aspect ratio. The aspect ratio is the number that results when the gap width between the cylinders is divided by the height of the cylinders. Taylor's theoretical results show that the flow between concentric rotating cylinders is always stable with respect to axisymmetric disturbances if the cylinders rotate in the same direction and the outer cylinder rotates faster than the inner. However, when the inner cylinder rotates faster than the outer, instabilities are predicted provided that the speed differential is sufficiently large. The form of the instability is one of steady counter-rotating toroidal vortices which encircle the inner cylinder and are uniformly spaced along the axis of rotation. Taylor also reported experiments which confirmed his stability analysis as well as the existence of the toroidal vortices which are now called Taylor vortices.

In later papers Taylor (3), (4), studied fluid friction and velocity profiles in the annular space. He concluded that the critical speed at which turbulence begins in the annular space is very much lower

for the case when the inner cylinder alone is rotating than for the case when the outer cylinder alone is rotating. The results further show that, when only the inner cylinder rotates, there are large velocity gradients confined to thin layers close to the walls, whereas when only the outer cylinder rotates there is a more nearly uniform velocity gradient throughout the space between the cylinders.

Investigations by Pai (5), for the case with only the inner cylinder rotating, showed that Taylor-type vortices also exist in turbulent flow at speeds several hundred times the critical speed as determined by Taylor's stability criterion.

Wendt (6) studied experimentally the case in which both cylinders rotate separately, with the liquid in the annulus having a free surface. Although the free surface may have had an influence on the observed turbulent velocity distributions, the results showed trends similar to those observed by Taylor. That is, when the inner cylinder rotated faster than the outer, the shear occurred near boundaries, whereas when the outer cylinder rotated faster than the inner, the velocity gradients were more nearly uniform throughout the annular space.

Coles (7) has made detailed observations of transition phenomena in the flow between two separately rotating concentric cylinders with the aid of visualization techniques and hot wire anemometry. His work includes the mapping of transition boundaries between the different modes of flow in great detail. It is particularly interesting to note that a strong hysteresis was found in the transition region in the case of the outer cylinder rotating.

From previous investigations it is thus known that Taylor-type vortices and the associated complication of the flow pattern can

be avoided if the outer cylinder is rotated faster than the inner. Furthermore, a turbulent velocity profile characterized by nearly uniform velocity gradients throughout the annulus can be expected. Therefore an apparatus for sediment studies was designed and built for this mode of operation. The apparatus consists of two concentrically rotating cylinders with end plates which rotate with the outer cylinder. The flow passage is then a continuous annular channel of rectangular cross-section in which the outer cylinder is analogous to the bed of an open channel. The handling of sediments and the manipulation of instruments in the annulus were deciding factors in the choice of the three inch gap width. The height of the cylinders is two feet,so that the aspect ratio is 1/8, which is slightly larger than the largest of three aspect ratios used by Wendt. It therefore came as a surprise when the first measured velocity profiles at mid-height showed an almost complete absence of shear throughout much of the gap width. So conspicuous is the absence of shear that a two inch thick layer of fluid adjacent to the outer cylinder wall moves with that wall in solid body rotation. It thus became clear, from these velocity measurements as well as from preliminary tests with sediments, that studies of sediment transport on the outer cylinder wall were not feasible with this equipment. It is, however, possible to study erosion and deposition processes on the inner cylinder wall provided the flow conditions there are known. It is for this reason that a theoretical and experimental study of the behaviour of homogeneous fluids was initiated in this system.

A preliminary study of the dynamics of the flow has indicated that the large aspect of the annulus is responsible for a strong

secondary flow during rotation, and that the momentum exchange occurs primarily between the inner cylinder surface and the end plates, thus causing the observed shearless region at the outer cylinder wall.

To develop an understanding of the mechanism for the unusual behaviour in the annular space, a laminar flow model was developed. The approach used is similar to that outlined by Greenspan (8), whereby a fluid, filling a container, rotates at a slight deviation from solid body rotation. The equations of motion are linearized by the elimination of some of the convective terms, which is justified following an order of magnitude comparison with the viscous terms. The fluid motion near the end plate is found to be of boundary layer character and involves a strong radial secondary motion. A similar analysis has been used by Wedemeyer (9) to describe unsteady flow in a closed cylindrical container.

The experimental objectives of the research are the observation of mean velocities, secondary motion, and turbulence structure. The information so obtained is to be used

1) as a comparison with the theory developed for laminar flow.
2) as a prerequisite to proposed studies of sedimentary processes near the inner cylinder.

The major portion of the observations were made with air as the test fluid using hot wire anemometers to observe turbulence and secondary motion as well as mean velocities.

CHAPTER II

THEORETICAL CONSIDERATIONS

2.1 Method of Solution

The difficulty in solving the Navier-Stokes equations is the presence of the non-linear convection terms in the momentum equations. However, a class of solutions of non-trivial flows does exist in which the convection terms conveniently vanish. For the equations in cartesian co-ordinates such solutions are generally obtained by setting all velocity components equal to zero except one. If u_1 is the non-zero velocity component, the continuity equation then implies that u_1 is independent of x_1. It then follows that all the convection terms vanish.

In cylindrical co-ordinates the laminar solution of circular Couette flow is similarly obtained by setting the radial velocity v_r and the axial velocity v_z equal to zero. This is permitted only when the cylinder axis has infinite length, making the flow independent of the axial co-ordinate so that v_z can be chosen equal to zero. When the length of the cylinders is finite, and in particular in the presence of end plates, the convection terms must be retained.

To define experimentally the shear field in the annular space of the rotating cylinders with end plates, velocity profiles in water were obtained at mid-height as shown in Fig. 1. In all runs the end plates are fixed to the outer cylinder. The striking feature of these profiles is the almost complete lack of shear throughout most of the gap width over a range of angular velocities of from 2.51 to 30.46 radians

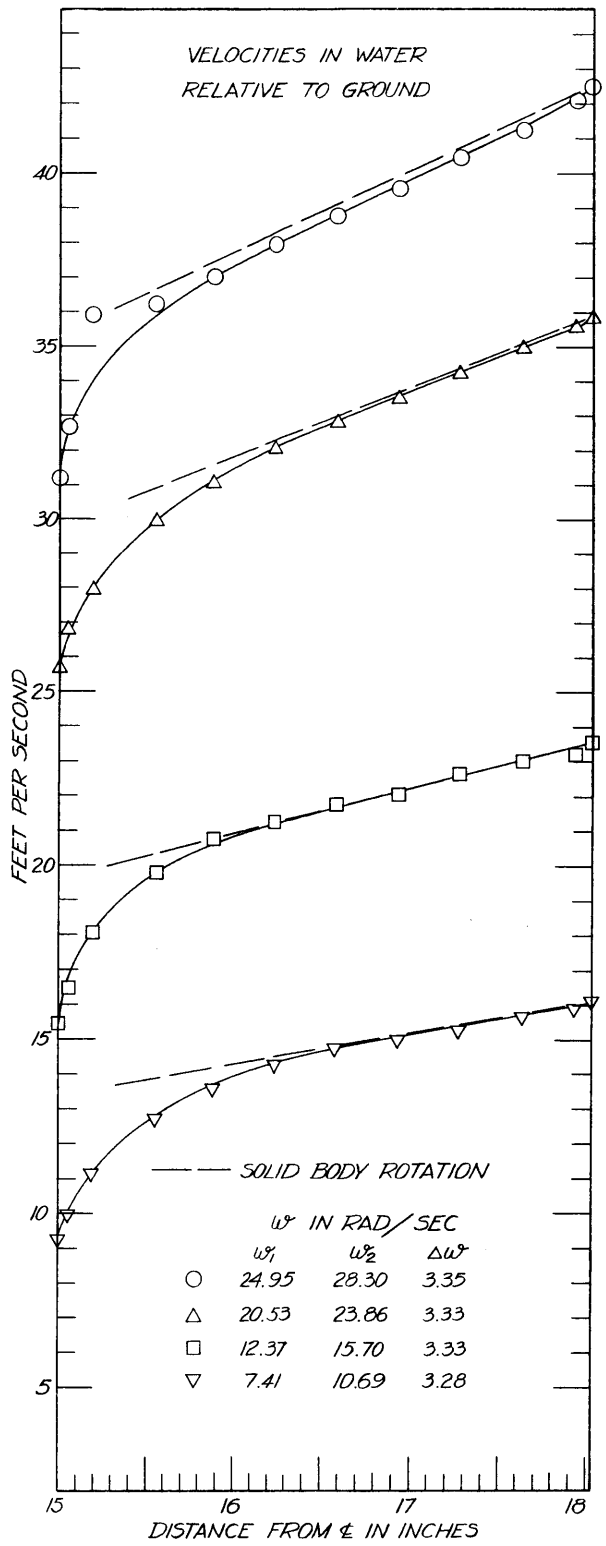

Absolute velocity profiles in water

Figure 1

per second. The fluid at mid-height therefore moves in solid body rotation with the outer cylinder, and it is only close to the inner cylinder wall that fluid shear becomes apparent.

At steady state there must be a balance between the moment of the shear force on the inner cylinder wall and that of the outer cylinder wall plus end plates. Since the shear force on the outer wall, at least at mid-height, is negligibly small, a strong shear force is expected at the end plates. This implies a large velocity gradient, and consequently the existence of a boundary layer at the end plates, with the fluid moving radially outward. Measured velocities near the upper end plate confirm this hypothesis that a strong secondary motion exists which is directed outward in the neighborhood of the end plates.

Continuity requires an inward flow away from the end plates and perhaps a second boundary layer at the inner cylinder surface in which the flow is toward the end plates as shown in Fig. 2. Turbulence measurements at mid-height have shown that throughout most of the gap width the intensities are low so that a laminar solution may have some success in representing the actual flow field. It is this model of nearly solid body rotation in the interior with a boundary layer at the end plates which serves as a basis for an analytical solution of the flow field in the annular space.

Consider the following argument: If both cylinders rotate at equal angular velocities, Ω, the flow field is identical to the forced vortex pattern. On the other hand, when the angular velocity of the inner cylinder is less than that of the outer cylinder by an amount $\Delta\Omega$, where $\Delta\Omega$ is smaller than Ω, a slight shear will be felt at

the inner cylinder wall. Using the ratio

$$\varepsilon = \frac{\Delta\Omega}{\Omega}$$

as the perturbation parameter, the solutions of the Navier-Stokes equations are developed as a perturbation of the state of solid body rotation. The procedure followed in developing these solutions is to identify the three important regions of the flow, as shown in Fig. 2. They are,

1) A boundary layer region near the end plate where the velocity changes rapidly with distance from the boundary.
2) A boundary layer region on the inner cylinder wall where the velocity changes rapidly with radial distance from that wall.
3) An interior region where the flow conditions are independent of the axial co-ordinate.

By an order of magnitude comparison of terms in the equations, separate solutions are obtained, first for the boundary layer type flow at the end plate, and then for the interior flow.

2.2 Perturbation Variables and Equations

The radial distance to any point in the annulus is expressed in terms of the radius, R, of the outer cylinder. In non-dimensional terms it takes the form

$$\eta = \frac{r}{R}$$

with $\alpha \leq \eta \leq 1$ where α is the ratio of the radii of the cylinders. Similarly, the non-dimensional axial co-ordinate can be written

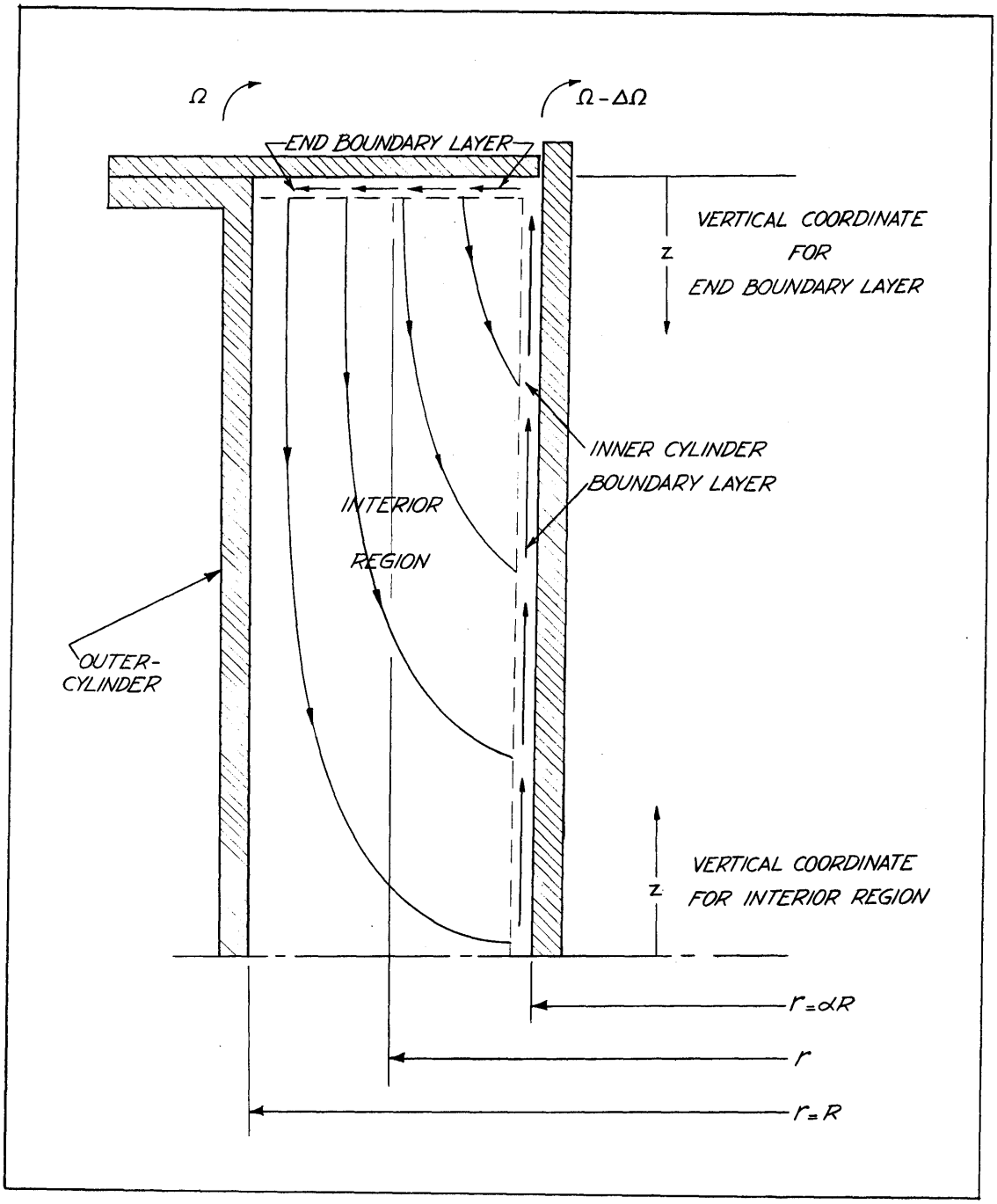

Qualitative secondary flow pattern in annulus

Figure 2

$$\xi = \frac{z}{h}$$

with $0 \leq \xi \leq 1$ where h is the axial scale of the motion.

The dependent variables, velocity and pressure, are represented as perturbation expansions in powers of the parameter

$$\varepsilon = \frac{\Delta\Omega}{\Omega} \tag{2.1}$$

as follows

$$\begin{aligned}
\frac{v_r}{R\Omega} &= \varepsilon u_1 + \varepsilon^2 u_2 + \ldots \\
\frac{v_z}{R\Omega} &= \frac{h}{R}\left(\varepsilon w_1 + \varepsilon^2 w_2 + \ldots\right) \\
\frac{v_\theta}{R\Omega} &= \eta - \left(\varepsilon v_1 + \varepsilon^2 v_2 + \ldots\right) \\
\frac{p}{\rho R^2 \Omega^2} &= \left(p_o + \varepsilon p_1 + \varepsilon^2 p_2 + \ldots\right)
\end{aligned} \tag{2.2}$$

The development presented here will deal with only the laminar flow case. The fluid will be treated as being incompressible, and it will furthermore be assumed that the cylinders are perfectly concentric so that the steady flow pattern will be rotationally symmetric. This permits elimination of the θ dependence in the continuity equation and in the Navier-Stokes equations, so that at steady state they can be written

<u>continuity</u>

$$\frac{1}{r}\frac{\partial}{\partial r}\left(\rho r v_r\right) + \frac{\partial}{\partial z}\left(\rho v_z\right) = 0$$

r component:

$$\rho\left(v_r \frac{\partial v_r}{\partial r} - \frac{v_\theta^2}{r} + v_z \frac{\partial v_r}{\partial z}\right) = -\frac{\partial p}{\partial r} + \mu\left[\frac{\partial}{\partial r}\left(\frac{1}{r}\frac{\partial}{\partial r}(rv_r)\right) + \frac{\partial^2 v_r}{\partial z^2}\right]$$

z component:

$$\rho\left(v_r \frac{\partial v_z}{\partial r} + v_z \frac{\partial v_z}{\partial z}\right) = -\frac{\partial p}{\partial z} + \mu\left[\frac{1}{r}\frac{\partial}{\partial r}\left(r\frac{\partial v_z}{\partial r}\right) + \frac{\partial^2 v_z}{\partial z^2}\right]$$

θ component:

$$\rho\left(v_r \frac{\partial v_\theta}{\partial r} + \frac{v_r v_\theta}{r} + v_z \frac{\partial v_\theta}{\partial z}\right) = \mu\left[\frac{\partial}{\partial r}\left(\frac{1}{r}\frac{\partial}{\partial r}(rv_\theta)\right) + \frac{\partial^2 v_\theta}{\partial z^2}\right]$$

These equations can be written in non-dimensional form by substitution of equations (2.2) and by the relations

$$\frac{\partial}{\partial r} = \frac{1}{R}\frac{\partial}{\partial \eta} \qquad (2.3)$$

$$\frac{\partial}{\partial z} = \frac{1}{h}\frac{\partial}{\partial \xi}$$

Including only the terms of zero order in ε the equations in non-dimensional form reduce to

r component:

$$\eta = \frac{\partial p_o}{\partial \eta}$$

z component:

$$0 = \frac{\partial p_o}{\partial \xi}$$

No zeroth order terms appear in the θ component. It can be readily verified that the zeroth order terms yield the basic solution,

$$v_r = v_z = 0$$

$$v_\theta = r\Omega$$

$$\frac{v_\theta^2}{r} = \frac{1}{\rho}\frac{\partial p}{\partial r}$$

Writing only the terms of first order in ε, the equations in non-dimensional form are,

r component:

$$-2v_1 = \frac{\partial p_1}{\partial \eta} - \frac{\nu}{R^2\Omega}\left[\frac{\partial}{\partial \eta}\left(\frac{1}{\eta}\frac{\partial}{\partial \eta}(\eta u_1)\right) + \frac{R^2}{h^2}\frac{\partial^2 u_1}{\partial \xi^2}\right] \tag{2.4}$$

z component:

$$0 = \frac{R^2}{h^2}\frac{\partial p_1}{\partial \xi} - \frac{\nu}{R^2\Omega}\left[\frac{1}{\eta}\frac{\partial}{\partial \eta}\left(\eta\frac{\partial w_1}{\partial \eta} + \frac{R^2}{h^2}\frac{\partial^2 w_1}{\partial \xi^2}\right)\right] \tag{2.5}$$

θ component:

$$2u_1 = -\frac{\nu}{R^2\Omega}\left[\frac{\partial}{\partial \eta}\left(\frac{1}{\eta}\frac{\partial}{\partial \eta}(\eta v_1)\right) + \frac{R^2}{h^2}\frac{\partial^2 v_1}{\partial \xi^2}\right] \tag{2.6}$$

The viscous terms in equations 2.4, 2.5, and 2.6 are all multiplied by the quantity $\frac{1}{E}$, where

$$E = \frac{R^2\Omega}{\nu} \tag{2.7}$$

The magnitude of this dimensionless quantity can be calculated for a given geometry when the angular speed and the fluid used are known. For the particular application in this report it is easily verified that

$$E >> 1 \tag{2.8}$$

2.3 End Boundary Layer Region

In light of previous discussion it is expected that the motion near the end plates will be of a boundary layer character. The axial scale h in the boundary layer is therefore considered to be small compared to the radial scale R. Consequently, terms multiplied by the coefficient R^2/h^2 tend to dominate terms multiplied by the coefficient of unity in the same non-dimensional equation. In the viscous part, therefore, of equations 2.4 through 2.6 it is permissible to neglect the first term as compared to the second. This transforms equations 2.4 through 2.6 into the first order boundary layer equations.

$$-2v_1 = \frac{\partial p_1}{\partial \eta} - \frac{1}{E}\left[\frac{R^2}{h^2}\frac{\partial^2 u_1}{\partial \xi^2}\right] \tag{2.9}$$

$$0 = \frac{R^2}{h^2}\frac{\partial p_1}{\partial \xi} - \frac{1}{E}\left[\frac{R^2}{h^2}\frac{\partial^2 w_1}{\partial \xi^2}\right] \tag{2.10}$$

$$2u_1 = \frac{1}{E}\left[-\frac{R^2}{h^2}\frac{\partial^2 v_1}{\partial \xi^2}\right] \tag{2.11}$$

In the previous section E was shown to be several orders of magnitude greater than unity. Consequently, from an order of magnitude comparison of the terms in equation 2.10 it can be seen that the pressure is independent of ξ to first order. The final end boundary layer equations can thus be written

$$2v_1 = \frac{1}{E}\frac{R^2}{h^2}\frac{\partial^2 u_1}{\partial \xi^2} - \frac{\partial p_1}{\partial \eta} \tag{2.12}$$

$$0 = \frac{\partial p_1}{\partial \xi} \tag{2.13}$$

$$2u_1 = -\frac{1}{E}\frac{R^2}{h^2}\frac{\partial^2 v_1}{\partial \xi^2} \tag{2.14}$$

We are required to match the interior solution to the end boundary solution at the latter's edge. If the non-dimensional first order circumferential velocity of the interior flow is denoted by $\bar{v}_1$, the pressure in the interior can be related to $\bar{v}_1$ from equation 2.4 using equation 2.8, and the condition that $\frac{R^2}{h^2}$ is of order unity in the interior. This results in

$$2\bar{v}_1 = -\frac{\partial \bar{p}_1}{\partial \eta} \tag{2.15}$$

From equation 2.13 it follows that the pressure in the boundary layer depends on η only and thus may be evaluated from the interior condition given by (2.15). Then from equation 2.12 it is evident that

$$2(v_1 - \bar{v}_1) = 2\hat{v}_1 = \frac{1}{E}\frac{R^2}{h^2}\frac{\partial^2 u_1}{\partial \xi^2} \tag{2.16}$$

For correct balance the terms in equation 2.16 are of equal magnitude. By equating the term $\frac{1}{E}\frac{R^2}{h^2}$ to unity, the scale of ξ in the boundary layer becomes fixed, thus yielding

$$h^2 = \frac{R^2}{E} = \frac{\nu}{\Omega} \tag{2.17}$$

Combining equations 2.14 and 2.16 results in a single differential equation for the tangential velocity as a function of the vertical

coordinate ξ,

$$\frac{\partial^4 \hat{v}}{\partial \xi^4} + 4\hat{v} = 0 \tag{2.18}$$

The subscript indicating that the velocity is of first order, has been dropped. It is noted that ξ is zero at the end plate, and positive in the direction of the interior.

Equation (2.18) must satisfy the following boundary conditions

$$\xi = 0,\ v_\theta = r\Omega = \eta R\Omega,\ v = 0,\ \hat{v} = \bar{v}$$

$$\xi = 0,\ v_r = 0,\ u = 0,\ \frac{\partial^2 v}{\partial \xi^2} = 0,\ \frac{\partial^2 \hat{v}}{\partial \xi^2} = 0 \tag{2.19}$$

$$\xi \to \infty,\ v \to \bar{v},\ \hat{v} \to 0$$

The solution of 2.18 satisfying the boundary conditions 2.19 is

$$\hat{v}(\eta,\xi) = -\bar{v}(\eta)e^{-\xi}\cos\xi \qquad \text{for } 0 \leq \xi < \infty \tag{2.20}$$

The distribution of the radial velocity in the boundary layer is obtained from 2.14

$$2u = -\frac{1}{E}\frac{R^2}{h^2}\frac{\partial^2}{\partial \xi^2}\left(-\bar{v}\, e^{-\xi}\cos\xi\right)$$

Using equation 2.17 we obtain

$$u(\eta,\xi) = \bar{v}(\eta)e^{-\xi}\sin\xi \tag{2.21}$$

Equations 2.20 and 2.21 exhibit velocity distributions in u and v which are similar to those of the classical Ekman layer (10). This velocity distribution is also found in a layer on the earth's surface

due to moving air masses. In this problem the flow outside the layer is characterized by a balance between the pressure field and the Coriolis forces. In the boundary layer the flow is decelerated causing a decrease in the Coriolis forces. A new balance is established between the pressure field, the diminished Coriolis forces, and the friction forces. The problem is discussed by Prandtl (11, p. 356) and was first formulated by Ekman. The present solution deviates from the classical Ekman layer in that the "inviscid" velocity vector is not constant but varies with η, thereby introducing a dependence on η in both $\hat{v}$ and u.

The radial discharge in the end boundary layer is

$$q = \int_0^\infty 2\pi r v_r dz \tag{2.22}$$

Using equations 2.2, 2.17 and the fact that $\xi = \frac{z}{h}$, the radial discharge after evaluation of the integral becomes

$$q = \pi r(\varepsilon \bar{v} R\Omega)\ (\nu/\Omega)^{1/2} \tag{2.23}$$

This discharge is written in dimensional form by using equation 2.2 for the term in brackets, which yields

$$q = \pi r(\nu/\Omega)^{1/2}\ (r\Omega - \bar{v}_\theta) \tag{2.24}$$

The boundary layer discharge is therefore a function of the thickness of the boundary layer $(\nu/\Omega)^{1/2}$, the radial distance itself, and the velocity differential between the interior flow and the end plate.

2.4 Interior Region

2.4.1. Interior Equations

In the interior the magnitudes of both R and h are of equal order so that in the equations 2.4, 2.5 and 2.6 we are not permitted to ignore terms multiplied by unity compared to terms multiplied by $\frac{R^2}{h^2}$. The relevant first order equations governing the flow in the interior written without subscripts thus are

$$2\bar{v} = \frac{1}{E}\left[\frac{\partial}{\partial\eta}\left(\frac{1}{\eta}\frac{\partial}{\partial\eta}(\eta\bar{u})\right) + \frac{R^2}{h^2}\frac{\partial^2\bar{u}}{\partial\xi^2}\right] - \frac{\partial\bar{p}}{\partial\eta} \tag{2.25}$$

$$0 = \frac{1}{E}\left[\frac{1}{\eta}\frac{\partial}{\partial\eta}\left(\eta\frac{\partial\bar{w}}{\partial\eta}\right) + \frac{R^2}{h^2}\frac{\partial^2\bar{w}}{\partial\xi^2}\right] - \frac{R^2}{h^2}\frac{\partial\bar{p}}{\partial\xi} \tag{2.26}$$

$$2\bar{u} = -\frac{1}{E}\left[\frac{\partial}{\partial\eta}\left(\frac{1}{\eta}\frac{\partial}{\partial\eta}(\eta\bar{v})\right) + \frac{R^2}{h^2}\frac{\partial^2\bar{v}}{\partial\xi^2}\right] \tag{2.27}$$

where the overbars denote that the variables pertain to flow conditions in the interior region. Using equation 2.8, it is evident from equation 2.26 that pressure is independent of ξ, and that equation 2.25 can then be written in the form

$$2\bar{v} = -\frac{\partial\bar{p}}{\partial\eta} \tag{2.28}$$

Since the pressure $\bar{p}$ is only a function of η, so is $\bar{v}$. Equation 2.27 therefore reduces to

$$2\bar{u} = -\frac{1}{E}\left[\frac{\partial}{\partial\eta}\left(\frac{1}{\eta}\frac{\partial}{\partial\eta}(\eta\bar{v})\right)\right] \tag{2.29}$$

from which it follows that $\bar{u} = \bar{u}(\eta)$.

From a continuity condition it is possible to write a relation between $\bar{u}$ and $\bar{v}$ in the interior region. Following a method used by

Wedemeyer (9), this relation is obtained from the coupling between the flows in the boundary layer and the interior. Thus radial inflow in the interior region must equal radial outflow through the boundary layer. The latter has been calculated and is given by equation 2.24. The former equals

$$q = 2\pi rH(-\bar{v}_r)$$

where H is the vertical distance from mid-height to end plate. Equating these discharges results in

$$\bar{v}_r = -\frac{1}{2}(\nu/H^2\Omega)^{1/2}(r\Omega - \bar{v}_\theta) \tag{2.30}$$

In terms of the perturbation variables defined in equation 2.2 this relation reads

$$\bar{u} = -\frac{1}{2}k\bar{v} \tag{2.31}$$

where

$$k = (\nu/H^2\Omega)^{1/2} \tag{2.32}$$

Now that it has been shown that $\bar{u}$ and $\bar{v}$ are functions of η alone, and that a unique relationship between these variables exists, it becomes possible to write equation 2.29 as a second-order, ordinary differential equation with either $\bar{u}$ or $\bar{v}$ as the dependent variable. We choose to write it for $\bar{v}$, giving

$$k\bar{v} = \frac{1}{E}\left[\frac{d}{d\eta}\frac{1}{\eta}\frac{d}{d\eta}(\eta\bar{v})\right]$$

After rearranging, this leads to,

$$\eta^2\frac{d^2\bar{v}}{d\eta^2} + \frac{d\bar{v}}{d\eta} - (1 + kE\eta^2)\bar{v} = 0 \tag{2.33}$$

The solution of equation 2.33 consists of modified Bessel functions of order one, expressing the tangential velocity $\bar{v}$ as a function of radial distance η. The general solution is

$$\bar{v} = c_1 I_1(\eta\sqrt{kE}) + c_2 K_1(\eta\sqrt{kE}) \tag{2.34}$$

2.4.2 Boundary Conditions and Solution

The general solution 2.34 must satisfy the following boundary conditions

$$\begin{aligned} &\eta = 1,\ \bar{v}_\theta = R\Omega,\ \ \bar{v} = 0 \\ &\eta = \alpha,\ \bar{v}_\theta = \alpha R(\Omega - \Delta\Omega),\ \alpha R\Delta\Omega = \bar{v}R\Delta\Omega,\ \bar{v} = \alpha \end{aligned} \tag{2.35}$$

It is obvious that at the inner cylinder wall $\bar{u} = 0$, and using equation 2.31, it is then also true that $\bar{v} = 0$. This is not compatible with the second boundary condition 2.35. This points out the necessity of a boundary layer flow at the inner cylinder wall.

This boundary layer has not been analyzed in detail, but order of magnitude considerations indicate that the change in the tangential velocity, v_θ, through this layer is very small. It is therefore assumed that the boundary condition 2.35 may be applied. Substitution in equation 2.34 yields two equations in the unknowns c_1 and c_2.

$$c_1 I_1(B) + c_2 K_1(B) = 0$$

$$c_1 I_1(\alpha B) + c_2 K_1(\alpha B) = \alpha$$

where $B = \sqrt{kE}$.

By Cramer's rule the solutions for c_1 and c_2 are

$$c_1 = \frac{-\alpha K_1(B)}{I_1(B)K_1(\alpha B) - K_1(B)I_1(\alpha B)} \tag{2.36}$$

$$c_2 = \frac{\alpha I_1(B)}{I_1(B)K_1(\alpha B) - K_1(B)\ I_1(\alpha B)} \tag{2.37}$$

The velocity at a given radius is thus a function of the quantities α, R/H and $E^{1/2}$. The first two quantities determine the geometry of the annular space while the last quantity is the square root of the dimensionless quantity which characterizes the Ekman layer.

2.4.3 Interior Solution for Large B

When the quantity $B = (kE)^{1/2} = [(R/H)(R^2\Omega/\nu)^{1/2}]^{1/2}$ is large compared to unity, the Bessel functions in the velocity equation can be expressed in terms of their asymptotic expansions,

$$\bar{v} \simeq c_1 \frac{e^{\eta B}}{\sqrt{(2\pi\eta B)}} + c_2\sqrt{\frac{\pi}{2\eta B}}\ e^{-\eta B}$$

Substitution of the boundary conditions 2.35, yields the approximate solution,

$$\bar{v} = \frac{\alpha\sqrt{\alpha}}{\sqrt{\eta}}\ \frac{\sinh B(1-\eta)}{\sinh B(1-\alpha)} \tag{2.38}$$

Since the geometry of the present apparatus is fixed, α, R and H are constant. The predicted shape of the velocity profile in the interior is thus dependent only on ν and Ω through B. Figure 3 shows variations in the predicted velocity profiles with the parameter B, as computed from equation 2.38.

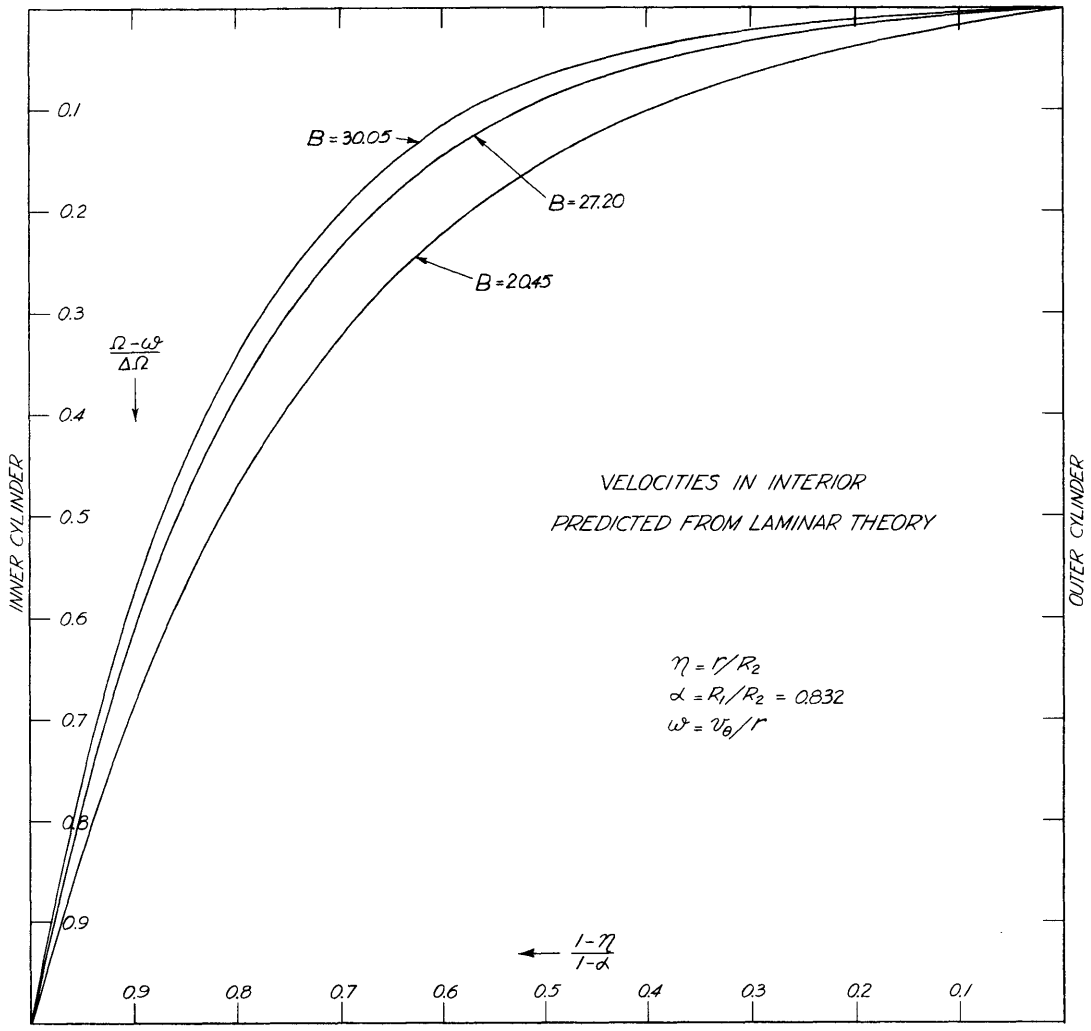

Predicted tangential velocities in interior region

Figure 3

2.4.4 Stream Function of the Interior Flow

The radial and vertical velocities in the interior of the annular space may be expressed in terms of the dimensionless Stokes' stream function

$$\bar{u} = -\frac{1}{\eta}\frac{\partial \psi}{\partial \xi} \tag{2.39}$$

$$\bar{w} = \frac{1}{\eta}\frac{\partial \psi}{\partial \eta} \tag{2.40}$$

Using equation 2.31, the stream function may be expressed in terms of the tangential velocity for which the distribution is known:

$$\psi = \frac{k}{2}\,\eta \int \bar{v}\, d\xi + f(\eta)$$

By substitution of equation 2.34 and noting that $\psi = 0$ for $\xi = 0$ the stream function is

$$\psi = \frac{k}{2}\,\eta\xi[c_1 I_1(\eta B) + c_2 K_1(\eta B)] \tag{2.41}$$

The stream function is a maximum for $\xi = 1$, $\eta = \alpha$

$$\psi_{max} = \frac{k\alpha}{2}\,[c_1 I_1(\alpha B) + c_2 K_1(\alpha B)]$$

The equation for the streamlines then becomes

$$\xi = \left(\frac{\psi\alpha}{\psi_{max}\eta}\right)\left[\frac{c_1 I_1(\alpha B) + c_2 K_1(\alpha B)}{c_1 I_1(\eta B) + c_2 K_1(\eta B)}\right] \tag{2.42}$$

The appropriate stream function for large B is obtained by a similar procedure. It can be shown to be

$$\psi = \frac{k}{2} \alpha\sqrt{\alpha} \sqrt{\eta} \xi \frac{\sinh B(1 - \eta)}{\sinh B(1 - \alpha)}$$

from which the streamline pattern is derived to give

$$\xi = \frac{\psi}{\psi_{max}} \sqrt{\frac{\alpha}{\eta}} \frac{\sinh B(1 - \alpha)}{\sinh B(1 - \eta)} \tag{2.43}$$

where

$$\psi_{max} = k\alpha^2/2 \tag{2.44}$$

Figure 4 shows the predicted streamline pattern in the interior for B held constant, as computed from equation 2.43.

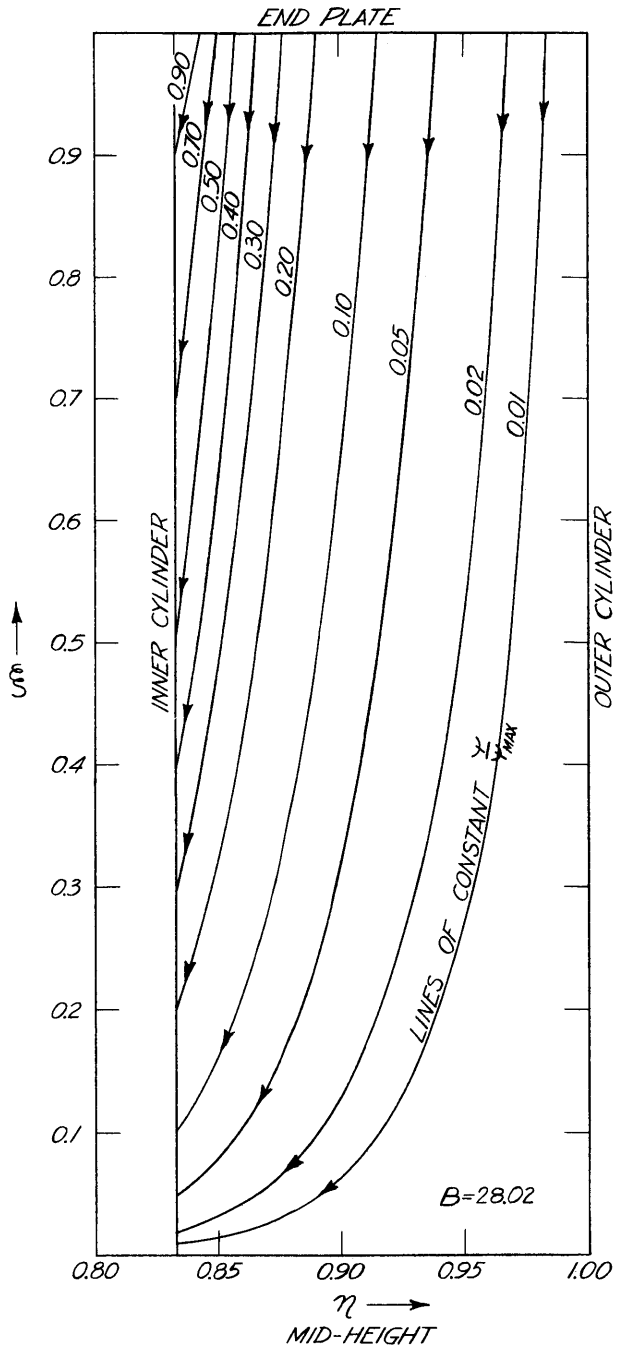

Predicted streamline pattern of secondary flow in interior region

Figure 4

CHAPTER III

EXPERIMENTAL ANALYSIS

3.1 Objectives and Design Conditions

The objectives of this phase of the research are directed toward collecting experimental data to be used

1) in a comparison with the laminar theory developed in Chapter II.
2) in constructing a complete flow pattern in the annular space so that sedimentary studies at the inner cylinder wall may be undertaken in a known flow field.

Experiments therefore include the measurement of velocity profiles, i.e., velocity magnitudes and directions, and turbulence intensities first at mid-height and later at different heights in the annular space. Flow direction and fluctuations in velocity are more easily measured in air with hot wire anemometry, so that hot wires are employed presently in this research. To obtain the direction of the velocity vector at varying axial locations throughout the gap width, X-array probes are to be used.

This phase of the research, covering the dynamics of homogeneous fluids in an annular space between rotating cylinders, is part of the sediment transport study. Consequently, the facility was not designed to specifically study homogeneous fluids. The design criteria for the methods of operation, control and measurements for the overall study are summarized in Report #83 of the Hydrodynamics Laboratory, Department of Civil Engineering, M. I. T. (12).

3.2 Description of Experimental Facility

3.2.1 The Main Apparatus

An assembled view of the apparatus is shown in Figure 5. The most important components are identified by a number in the sketch. Items 4 and 5 are the co-axial cylinders forming the annular flow passage. This annular space is closed above by an end plate, 8, made of acrylic plastic, bolted to the outer cylinder. The bottom plate, 6, which supports the outer cylinder is attached to a hollow outer shaft, 2, which transmits its load to a tapered roller thrust bearing, 13, mounted on the rigid frame. Concentric rotation of the cylinders is achieved by two radial ball bearings between the outer and inner shafts. The inner shaft, supporting the inner cylinder by means of four arms, transmits its vertical load to the frame by means of a thrust bearing, 13. The cylinders are separately driven by 1.5 HP D.C. motors at speeds of up to 300 rpm through notched belts and pulleys. Separate speed control of each motor is achieved by a General Electric Amplidyne in a closed loop with a tachometer-generator, driven directly by the motor. The control system, which uses an external D.C. reference voltage, is shown in Figure 6. To inhibit rust formation and corrosion, all supporting members in contact with the test fluid are made of type 316 stainless steel. The cylinder walls and flanges were fabricated from 1/2 inch plate, and all welds were annealed prior to machining. Bronze parts were used where mechanical strength is less critical. The final dimensions of the annular gap measure 15.000 inches inner diameter and 18.017 inches outer diameter. The cylinder surfaces are machined to a tolerance of $\pm$ 0.010 inches, limiting cross-sectional variations in the radial direction to less than 0.35%. The distance between the top

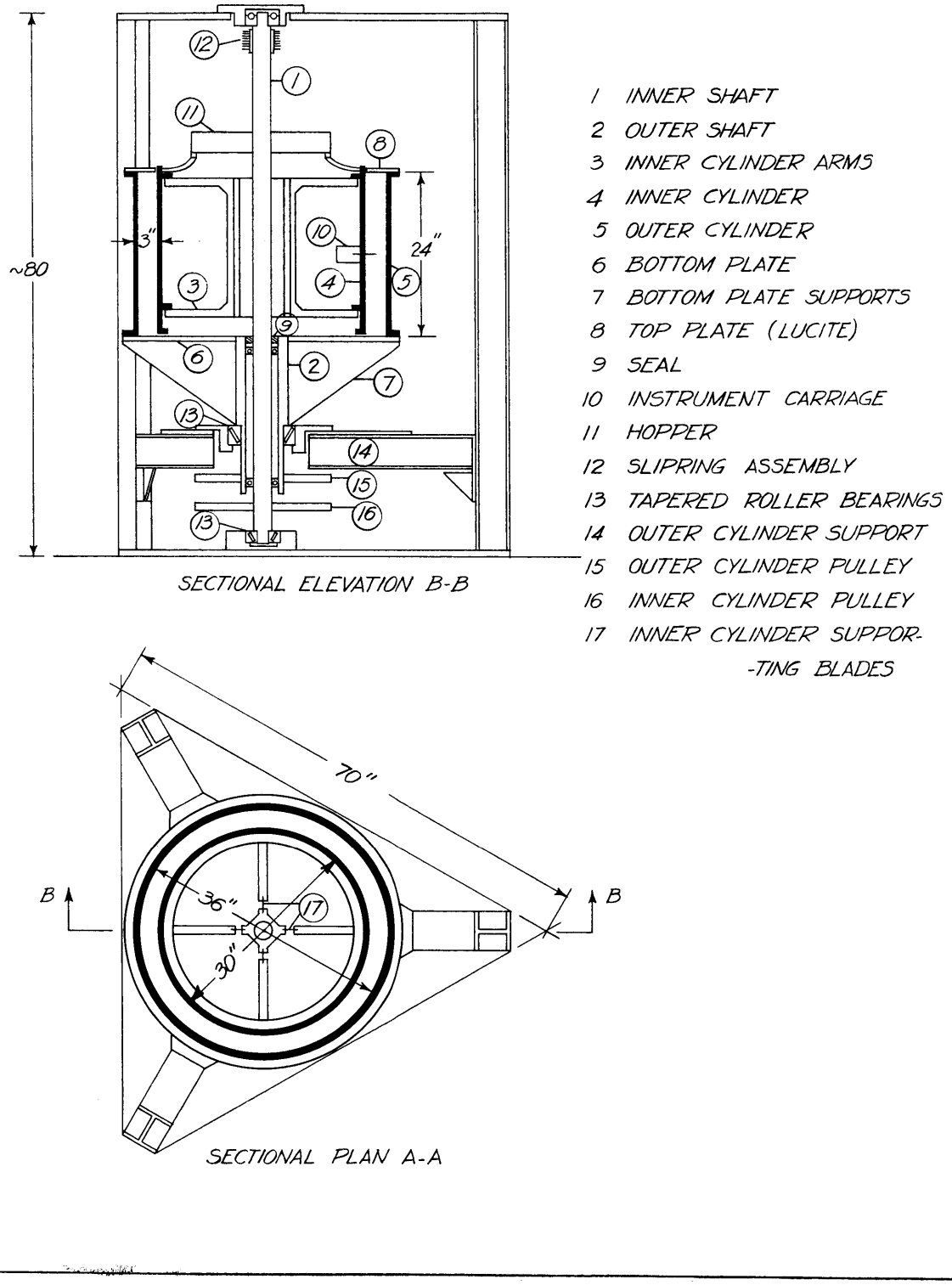

Assembled view of rotating cylinders

Figure 5

and bottom plates is 24 inches with an estimated variation of 0.2%.

3.2.2 Instrumentation

Speed measurement - The determination of rotational speed is extremely critical because the centripetal acceleration varies as the square of the angular velocity. Values computed for the radial pressure gradient are therefore sensitive to small errors in the measured speed of rotation. Because the cylinders are coupled to the motors through positive drive belts, speed can be accurately measured on the motor shafts. A perforated disk mounted on each motor shaft interrupts a light beam focussed on a photocell. The output of the photocell is counted electronically, giving the speed to a precision of 1/500, over the entire range of operation.

Sliprings - To allow control signals and measured signals to be transmitted into and out of the apparatus while the cylinders are rotating, a set of mechanical slipring consisting of 18 information channels was used. These sliprings proved to be electrically noisy and were used only for the transmission of control signals such as those required to drive the traversing mechanism carrying the pitot static tube. For the transmission of signals from hot wires a set of mercury sliprings was devised which proved to be noise-free. The mercury is contained in a set of stationary annular reservoirs as shown in Figure 7, into which circular electrodes, rotating with the inner cylinder, are immersed. Eight such channels are presently in use. Due to vibration in the apparatus, ripples or waves are introduced on the surface of the mercury. To avoid any possible electrical noise from the surface irregularities in the mercury, the brass

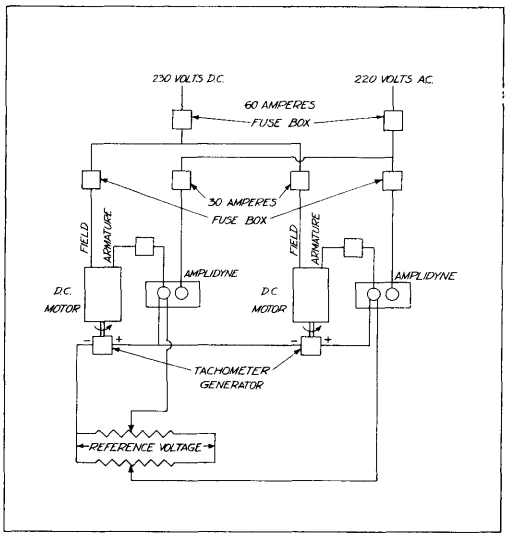

Figure 6 - Cylinder speed control system

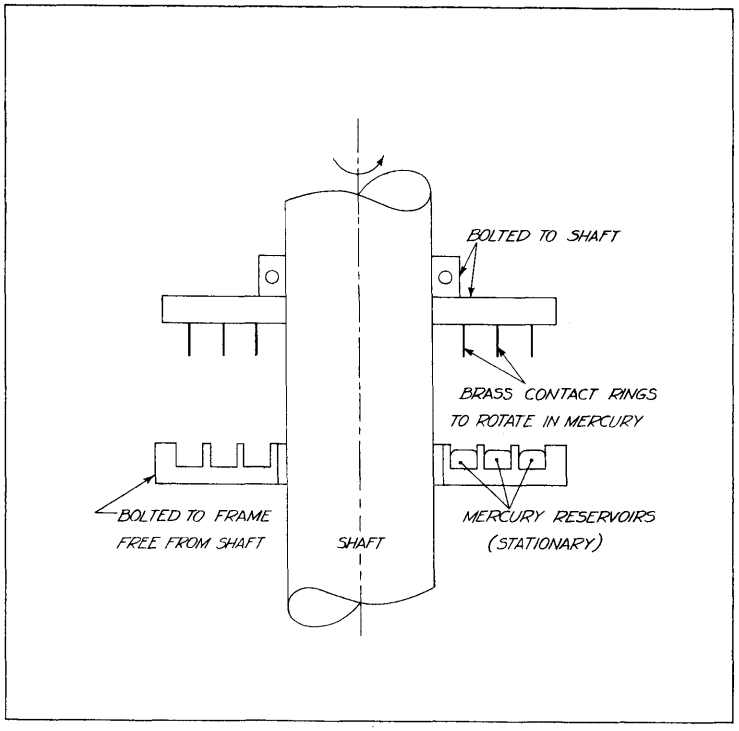

Figure 7 - Mercury slipring assembly

electrodes were coated with a spray enamel and only the bottom edge is allowed to make contact with the mercury. The resistance of this type of slipring is negligibly small and it is noise-free at all angular speeds tested.

Pitot Static Tube - Velocity profiles in water were obtained at mid-height of the annular passage with a pitot static tube, as shown in Figure 8, through an opening in the inner cylinder wall. The support and traversing mechanism, shown in Figure 9, allows movement and accurate placement of the instrument while the cylinders are rotating. A small D.C. motor which drives the probe lead screw, is also coupled to a rotary potentiometer. The resistance of this potentiometer, which forms one leg of an external Wheatstone bridge circuit, was calibrated to give the position of the probe. Figure 9 shows the pressure leads from the probe connected to a differential pressure transducer. Pressure measurements using this transducer proved unsuccessful due to excessive vibration pick-up by this extremely sensitive instrument. Instead, a differential manometer mounted on the hub of the inner cylinder was used. A stroboscope, mechanically synchronized with the inner cylinder, served to illuminate the rotating manometer. Readings were taken with a transit telescope. In setting up such a manometer it is extremely critical that the tubes be vertical and equidistant from the axis of rotation. Although the menisci are sloping during rotation, they are clearly visible and it was found that readings can be adequately reproduced provided the tubes and manometer fluid are kept clean.

Hot wire anemometer - Mean and fluctuating velocities

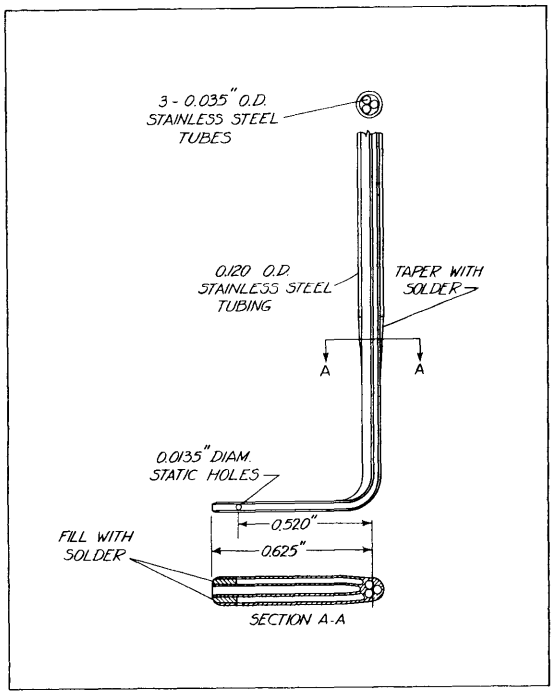

Figure 8 Impact tube

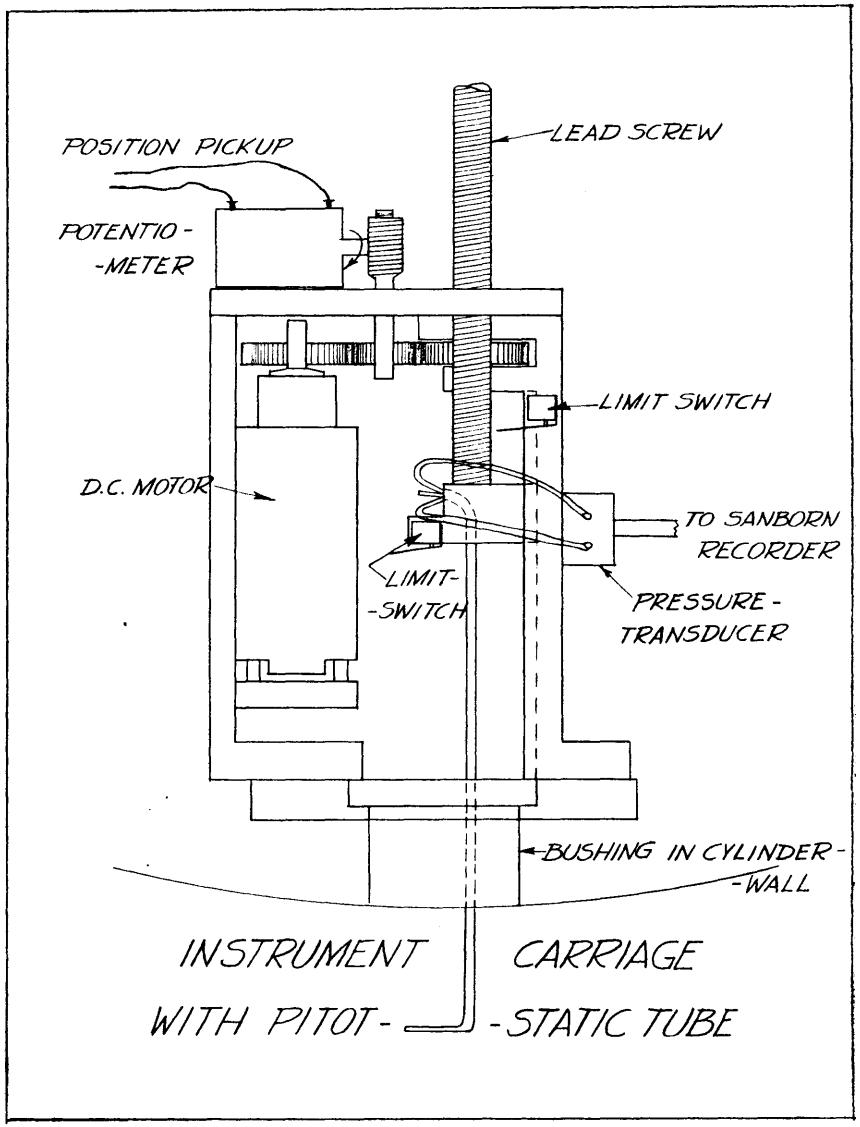

Figure 9 Traversing mechanism for velocity probes

in air are obtained at mid-height with hot wire probes (Figure 10) operated at constant temperature with a Thermo Systems Model 1020-A Bridge Amplifier and a Flow Corporation Model CTA-3 Bridge Amplifier. The hot wire probe is mounted in the opening in the inner cylinder wall, without the use of a traversing mechanism, and is moved manually into the desired radial position. The calibration of these probes was done in a 2 inch diameter acrylic plastic pipe approximately 4 inches downstream from a bell-shaped inlet. The 9 inch diameter stilling chamber upstream from the inlet is 20 inches long and contains 4 inch long tubular flow straighteners at the upstream end to ensure uniform small scale turbulence throughout the cross-section. The resulting velocity profile at the test section was uniform.

The electrical power supplied to the hot wire is calibrated against a known velocity. Calibration of hot wires as well as calculations of turbulence intensities are discussed in Appendix B. The known velocity is obtained from an average of four velocity measurements, one of which is obtained from a Venturi meter, with a diameter ratio of 2, located downstream from the test section. The pressure differential is read by means of a micromanometer. It was found that during the calibrations the air blower was unsteady at low discharges. The lowest discharge judged sufficiently steady corresponded to a pressure differential of 0.01 inches, which represents a velocity of approximately 1.3 fps. The other three velocity measurements were obtained indirectly by observation of the frequency of vortex shedding from a stationary cylinder (see, for instance, ref. 13). Three different sizes of rods were used in the calibration. The relationship between the dimensionless shedding

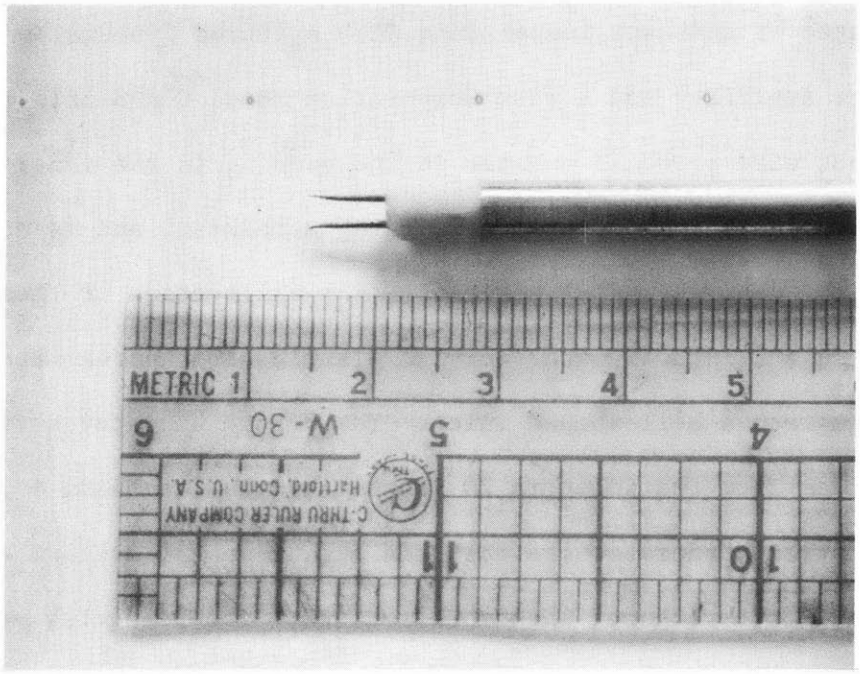

0.00035" tungsten hot wire anemometer

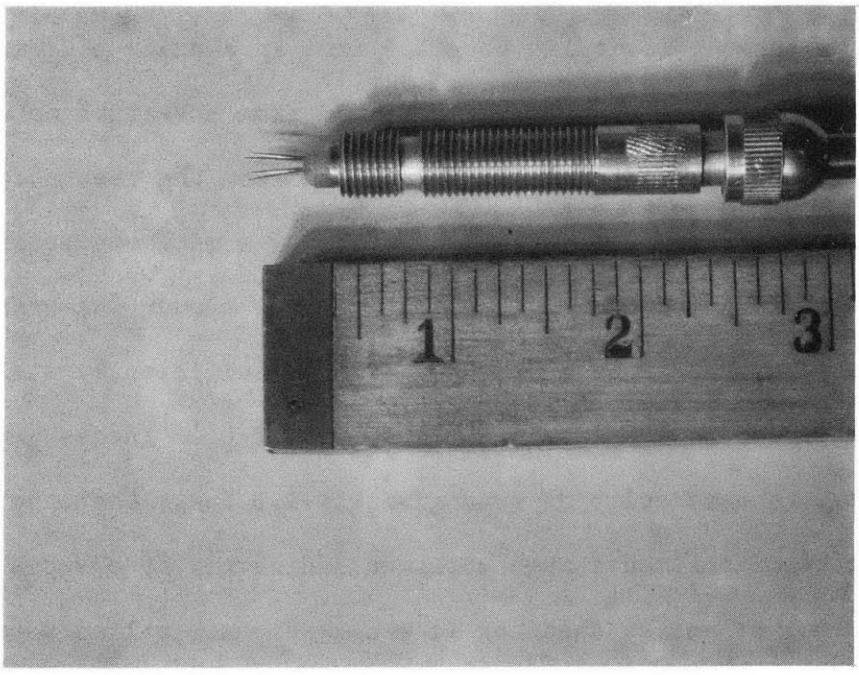

X array anemometer with 0.00035" tungsten wires

Figure 10

frequency (Strouhal number) for a circular cylinder and Reynolds number served as a means to convert frequency to air velocity.

3.3 Experimental Methods

3.3.1 Preliminary Tests

Test with water - The velocity field in the annular space can be assumed to be vertically symmetric about a horizontal plane at mid-height only when the annulus is completely filled with water. At rest, water fills the inner cylinder as well as the annular space to a common level. During rotation, however, the centrifugal acceleration forces part of the fluid into the annular space. Consequently, the higher the angular speeds, the more fluid is forced into the annular space so that for any given volume of water in the apparatus an angular speed exists for which the annulus is filled. Increasing the angular speed further will cause spillage from between the top plate and the inner cylinder wall. Volume changes are thus necessary whenever the angular speeds are changed. At higher angular speeds of 250 to 300 rpm, however, the centrifugal acceleration approaches values of 40 gravities causing a slope of 40 to 1 in the piezometric surface. Under these conditions small changes in angular speed have little effect on the slope of the piezometric surface in the annular space, making volume changes unnecessary. The correct volume for each desired angular velocity combination was obtained by trial runs. A mark was made on the inner cylinder wall to indicate the required water level for a particular speed combination. For all test runs the still water level fell below mid-height of the cylinders, which necessitated a procedure for de-airing the pitot static tube located at mid-height. By rotating the outer

cylinder alone the centrifugal acceleration forced the fluid outward, thereby raising the level in the annular space and submerging the probe. With the inner cylinder, and thereby the probe and manometer, at rest the system was de-aired.

Test with air - When air is used as the test fluid in the annular space, volume adjustments as required with water are not necessary. However, another problem arises, which can best be visualized as follows: Consider a given volume of water in the apparatus when it is at rest. From an argument analogous to that of the previous section a combination of angular speeds can be found for which the annulus is just filled with water. Adding more water to the inner cylinder at this "equilibrium" speed causes spillage from between the top plate and the inner cylinder wall, since the piezometric surface is raised. A continuous through-flow will therefore result if an unlimited supply of water is available to the inner cylinder. This condition may also prevail when air is used as the test fluid. Preliminary tests with hot wire probes have indicated that a through-flow does exist. Attempts to seal the opening between the top plate and the inner cylinder failed. At present, through-flow is prevented by a seal in the bottom part of the apparatus as shown in Figure 11. An annular rubber strip is attached between a horizontal flange on the inner cylinder, and a circular steel ring which rotates with the inner cylinder. A 1/16 inch thick teflon strip glued to the bottom of the ring provides for a smooth sliding contact between the ring and the bottom plate. The ring is centered by means of four brackets mounted on the inner cylinder each having an adjustment screw which exerts pressure on the inside of the ring.

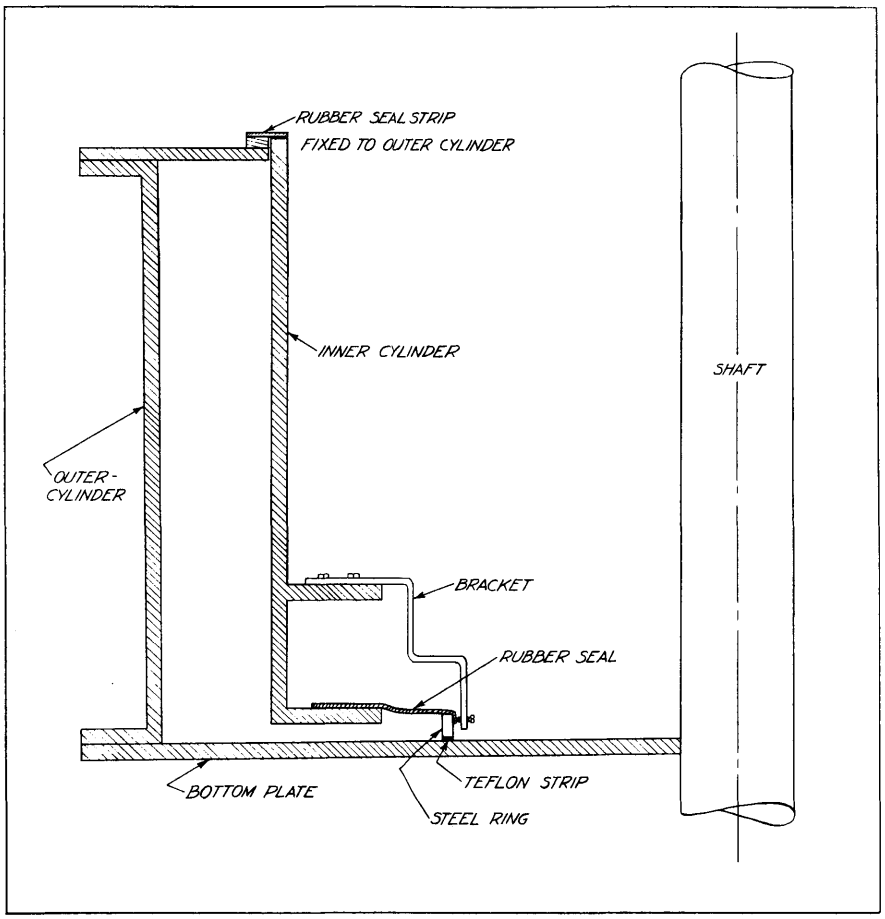

Air seal for prevention of axial flow

Figure 11

Aside from the problem of through-flow, the early velocity profiles with the single hot wire probe were not reproducible. This was primarily due to a drift in the initial current I_o (see Appendix B), which caused a change in the calibration equation,

$$I^2 = I_o^2 + B\sqrt{U}$$

Note that a plot of I^2 versus $\sqrt{U}$ produces a straight line with intercept I_o^2. It was found that the variation of I_o^2 could be accounted for by rewriting the calibration equation in the form

$$\frac{I^2 - I_o^2}{I_o^2} = \frac{B}{I_o^2}\sqrt{U}$$

A plot of $(I^2 - I_o^2)/I_o^2$ versus $\sqrt{U}$ thus yields a straight line which passes through the origin. Calibration curves as well as velocity profiles were found to be reproducible using this method of plotting.

Various sizes of hot wires were used in the collection of experimental data. The size that best suited our requirements for both the single wire and X-array probes was the 0.00035 inch diameter platinum or tungsten wire. It is relatively sturdy, and has a good frequency response in the range from 0 cps to 15,000 cps at zero velocity. It is therefore capable of measuring turbulent velocity fluctuations. The X-array probe has two single wires mounted in the form of an X. The wires are separately supported and each is operated by a different bridge amplifier, so that each signal can be monitored on an oscilloscope. It can be shown (14) that a single hot wire is most sensitive to direction when it makes an angle of 45° with the direction of flow. It is for this reason that the X-array probe, in which both wires are approximately at 45° to the flow, is well suited for direction measurements.

By displaying the output from the bridge amplifier on an oscilloscope, a study of the structure of turbulence is possible. In this manner it was observed that at all angular speeds a recurring signal, which was periodic with the inner cylinder, occurred. Observations with both cylinders locked together, so that there is no air movement relative to the cylinders, produced the same periodic signal. The cause of this periodic signal is not understood. It is presently under

investigation. The influence of the periodic signal on the observations of mean velocity can be considered negligible because the tangential velocity fluctuations $\left(\overline{v_\theta'^2}\right)^{1/2}$ were at most 25 per cent of the local mean velocity (see Appendix B).

The possibility that the hot wire probe is measuring its own wake when it is used in the rotating annular space was investigated. A dummy probe of identical size as the recording probe was inserted into the annular space at a location diametrically across from the active probe. The observed mean current and the root mean squared value of the voltage signal supplied by the Bridge Amplifier to the recording probe were measured for the dummy probe inserted and removed. No measurable differences between the outputs were found.

3.3.2 Velocities in Water

The velocities in water were measured with the pitot static tube which was mounted through the inner cylinder wall and connected to a differential manometer which was also rotating with the inner cylinder. Velocity profiles were obtained by selecting a desired angular speed for both cylinders, and then making a traverse with the pitot static tube starting at the inner cylinder wall in steps of one eighth to one quarter inch.

Because of space considerations and ease of reading, the length of the manometer was limited to 18 inches. To cover the required range of velocities with this size of manometer the indicating fluid selected was #3 Merriam fluid with a specific gravity of 2.95. To obtain reliable differential pressure readings from this manometer it is

of paramount importance that the manometer tubes be vertical and parallel and that they are equidistant from the center of rotation. To check these conditions the cylinders were rotated together at various angular speeds after de-airing the pitot static tube. Since the velocities relative to the probe then are zero, the manometer must read a zero differential. Many velocity measurements were discarded because of trapped air in the system.

To be certain that steady state conditions prevail, a certain spin-up time must be allowed after the cylinders have attained the required angular speeds. Since each velocity profile in water was obtained for a given set of angular speeds, the spin-up time was important only for the first readings. Greenspan and Howard (15) have indicated that the spin-up time required in a single container is of the order of $T = L(\Omega\nu)^{-1/2}$ seconds, where L is a characteristic length of the container. To get an idea of the order of magnitude of the spin-up time, the above formula was used. Using a characteristic length of one foot, the spin-up amounts to 182 seconds for an angular velocity of 2.51 rad/sec, whereas only 52 seconds are required for an angular velocity of 30.46 rad/sec. In air these values are reduced to approximately one third of the above values due to the increase in the kinematic viscosity. This indicates that for both types of measurements the spin-up time is unimportant.

3.3.3. Velocities in Air

Mean velocities and velocity fluctuations at mid-height were obtained by observing the mean heating current and the root mean square of the fluctuating voltage, respectively, which were required to keep the hot wire anemometer in the flow at a constant temperature. For

each radial position of the probe in the annular space, the speeds where varied to give the same speed conditions as obtained in the tests using water. In the previous section it was shown that the spin-up time required in air is small and may be considered unimportant. The previously mentioned periodic signal may contribute to the value of the rms of the voltage and a correction may be necessary for the computation of the turbulence intensities. In this report, however, all turbulence data are presented in uncorrected form since it is still uncertain what correction should be applied.

3.4 Analysis of Data

In the calibration of the hot wire anemometer, a number of correction procedures were used. They were instrumental in producing reproducible mean velocities during the calibration procedures. The known velocity from which the hot wires were calibrated was an average of four velocity measurements, three of which were obtained from a Strouhal-Reynolds number relationship, and the remaining one was obtained from a Venturi meter.

For the determination of velocity from the frequency of vortex shedding, the following relationships (16) were used:

$$S = 0.212 \left[1 - \frac{21.2}{Re}\right] \qquad 40 < Re < 150$$

$$S = 0.212 \left[1 - \frac{12.7}{Re}\right] \qquad 300 < Re < 5000$$

where $S = fd/U$ is the dimensionless frequency or Strouhal number

$Re = Ud/\nu$ is the Reynolds number

d = the diameter of the shedding rod.

For Reynolds numbers between 150 and 300 a linear relationship, joining the curves defined by the above relations, was assumed. Three different sizes of rods were used for the shedding of vortices. The output from the hot wire anemometer positioned in the vortex street was displayed on an oscilloscope, and the frequency of shedding was counted with an electric counter. It was found that the velocities computed from the shedding frequencies of three different rod sizes agreed within one half per cent. It is noted here that it is important that the shedding rods extend from wall to wall in the circular cross-section. The frequency of shedding was altered by more than ten per cent, for instance, in a 3 x 4 inch rectangular wind tunnel when a 1/8 inch diameter shedding rod was moved away a distance of 1/8 of an inch from one of the walls.

The velocities obtained from the above procedure were compared with those obtained from a Venturi meter with a diameter ratio of 2 connected to a micromanometer. After correction of the computed velocity from the Venturi meter by a discharge coefficient, using a table by Rouse (17), the agreement obtained was within one half per cent. The velocities so obtained were used as the known velocity in the hot wire calibration procedure. Since the shedding rods reduce the effective cross-sectional area of the 2 inch diameter test section, an area correction coefficient was applied to account for the resulting change in velocity.

A computer program was written in which these correction procedures were incorporated. A copy of this program is included in Appendix C.

Mean velocities in the annular space were computed from the

observed mean heating current to the hot wire, using equation 5 in Appendix B, where the constants I_o^2 and B were obtained from the calibration of the hot wire anemometer. The turbulence intensities were calculated, using the linear relationship of equation 6 in Appendix B. A computer program was written to perform the required operations in calculating mean velocities and turbulence intensities. A sample program is included in Appendix C.

For the plotting of the predicted velocities and streamline patterns in the interior region of the annular space, a third computer program was written. Velocities and ψ-co-ordinates are calculated at intervals of 1/4 of an inch across the annular space, using equations 2.38 and 2.43 respectively. The ordinate in the velocity diagrams, $\frac{\Omega - \omega}{\Delta\Omega}$, is written in terms of the velocity, v, expressed in the above equations by recalling that the perturbation velocity is written $v_\theta = (r\Omega - \varepsilon v R\Omega)$. A few points were calculated from the exact solutions, equations 2.34 and 2.42, and compared with the solutions obtained by the asymptotic expansion, equations 2.38 and 2.43. The largest discrepancy in the velocity between the two solutions is expected at small values of Ω. This discrepancy was approximately one per cent at Ω = 2.51 rad/sec. The solution using the asymptotic expansion was thus used throughout.

The computer program which performs the detailed operations in the calculation of tangential velocities and streamline co-ordinates is listed in Appendix C.

CHAPTER IV

DISCUSSION OF RESULTS

The observed mean velocity profiles at mid-height are presented in Figures 12 through 15. Figures 12 and 13 show the experimental velocity profiles in water compared with those predicted from the laminar theory. Figures 14 and 15 show the same comparison when the test fluid is air. In all these figures the co-ordinate system has been selected such that experimental data collected from apparatus with different geometry can be compared in the same plot. This has the advantage that the influence of various factors such as total angular velocity Ω, aspect ratio, the ratio $\varepsilon = \frac{\Delta\Omega}{\Omega}$, viscosity or possibly the eddy viscosity can be detected by merely observing the shape of the velocity profile.

The ordinate in these plots is taken to be an angular velocity defect from the angular velocity Ω of the outer cylinder in non-dimensional form. This means that when the fluid is in a state of solid body rotation with the outer cylinder, the local angular velocity is everywhere equal to Ω, so that the angular velocity defect is then zero. Therefore, the horizontal line with ordinate equal to zero is identified with the distribution of velocity when the fluid is in solid body rotation with the outer cylinder. The no slip condition requires that all velocity profiles originate at the point of zero ordinate at the outer cylinder wall. In the figures, this is the point in the top right hand corner. At the inner cylinder wall the angular velocity defect is at its maximum value of $\Delta\Omega$. In non-dimensional form the ordinate there is thus equal to unity, so that all velocity profiles must intersect the inner cylinder wall at the point where the ordinate is equal to unity. This point

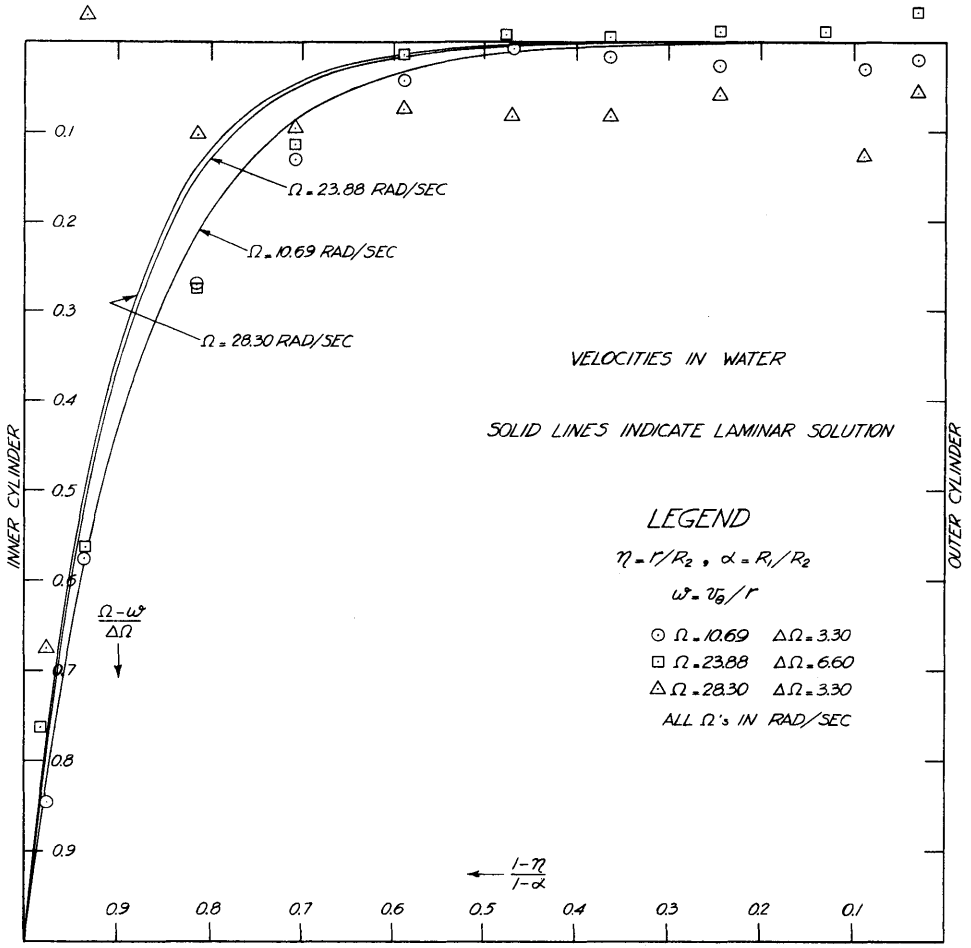

Tangential velocities in water

Figure 12

corresponds to the lower left hand corner of the diagram. The abscissa for each plot, which represents the radial co-ordinate, is the variable $(R_2 - r)/t$ where $t = (R_2 - R_1)$ is the distance between the cylinders. The predicted tangential velocities from the laminar theory are shown in Figure 12 as solid curves for three values of angular velocity Ω. These curves are, of course, similar to those presented previously in Figure 3, and indicate the influence of the total rate of rotation on the shape of the tangential velocity profile. The higher the rate of rotation the more closely the tangential velocity distribution approaches that of solid body rotation. The observed velocities are also shown in Figure 12. It is noted that the experimental velocity profiles have the same general shape at the predicted ones. There is, however, considerable scatter in the experimental data, so that detailed comparisons with the theory are not meaningful. Much of this scatter may be due to difficulties in reading the differential manometer, in particular at higher angular velocities when the slope of the meniscus is large.

Another set of velocity profiles in water with lower angular velocities is shown in Figure 13. The upper set of solid curves is again the predicted tangential velocities from the laminar theory, whereas the solid lines marked "modified solution" indicate predicted tangential velocities when the kinematic viscosity ν is replaced by an eddy viscosity ν_t. The eddy viscosity is introduced to indicate the general influence of turbulence on the mean velocity profiles. Curves are shown for values of ν_t/ν of 20 and 50. The trend in the curves indicates that an increase in viscosity tends to increase the defect of angular velocity from that of the outer cylinder. This is due to the dependence of the predicted tangential velocity on the ratio $\sinh B(1 - \eta)/\sinh B(1 - \alpha)$

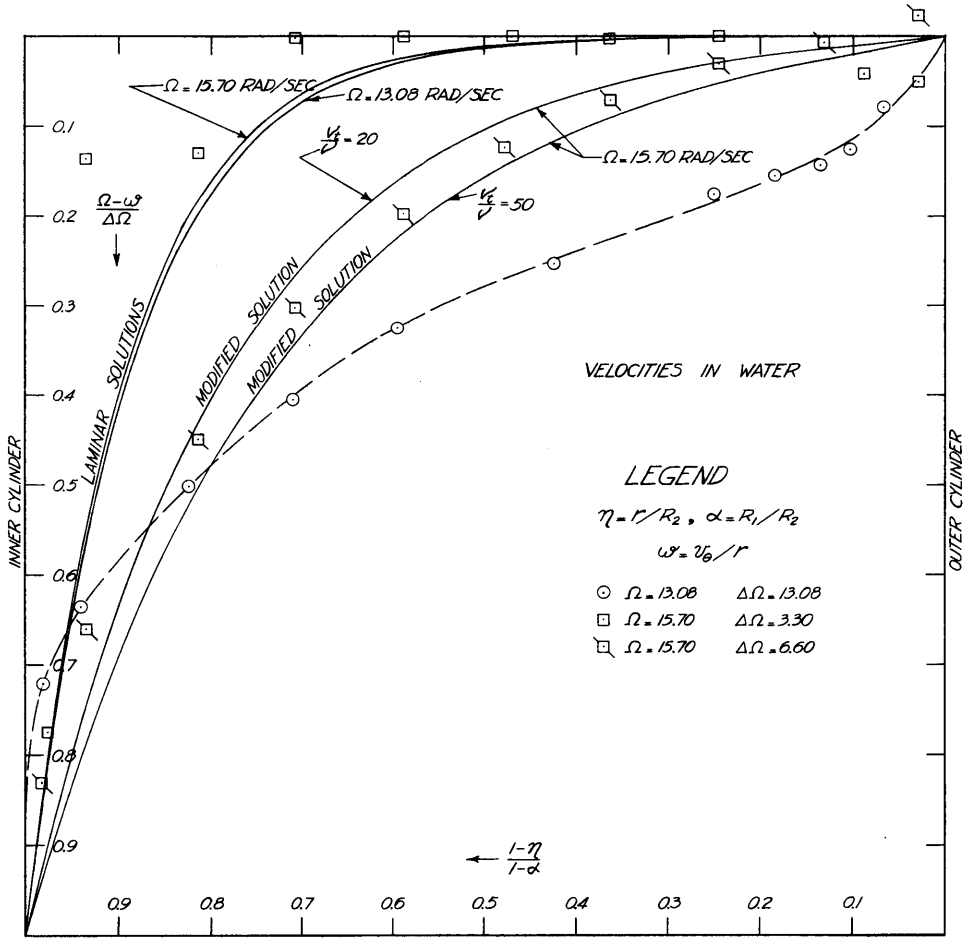

Tangential velocities in water

Figure 13

as expressed in equation 2.38, in which B varies inversely as the fourth root of the viscosity. It is noted that the eddy viscosity has been assumed constant throughout the width of the annular space.

The observed tangential velocities shown in Figure 13 indicate, from a comparison of the two profiles that Ω = 15.7 rad/sec, that contrary to results in Figure 12, a change in $\Delta\Omega$ has a notable effect on the shape of the measured velocity profiles. It is evident for instance that although the data for $\Delta\Omega$ = 3.30 rad/sec show more scatter, they produce a velocity profile which resembles the predicted curve more closely than the data for $\Delta\Omega$ = 6.60 rad/sec. Although this behaviour is not predicted by the laminar theory it should be noted that the theory is restricted to flows in which $\varepsilon = \Delta\Omega/\Omega$ is small compared to unity. It is possible that a change in $\Delta\Omega$ and therefore in ε is difficult to detect when the magnitude of ε is smaller than 0.27 as it is in Figure 12.

An increase in $\Delta\Omega$ is analogous to an increase in the Reynolds number if the latter is defined as $Re = \Delta\Omega Rt/\nu$. Intuitively an increase in Reynolds number will increase the turbulent mixing. It is thus possible that the turbulence level is significantly increased at $\Delta\Omega$ = 6.60 rad/sec, in which case it would be reasonable to introduce the eddy viscosity. It is seen from Figure 13 that there is reasonable agreement between the "modified solution" and the data at $\Delta\Omega$ = 6.60 rad/sec if the eddy viscosity is taken between 20 and 50 times the kinematic viscosity. The remaining set of data in Figure 13 are for the inner cylinder fixed, in which case $\varepsilon = \Delta\Omega/\Omega = 1$ so that the theory is not expected to be applicable. The velocity here resembles more closely a shear profile such as has been observed by Taylor (3) and Wendt (6) in systems with smaller aspect ratios.

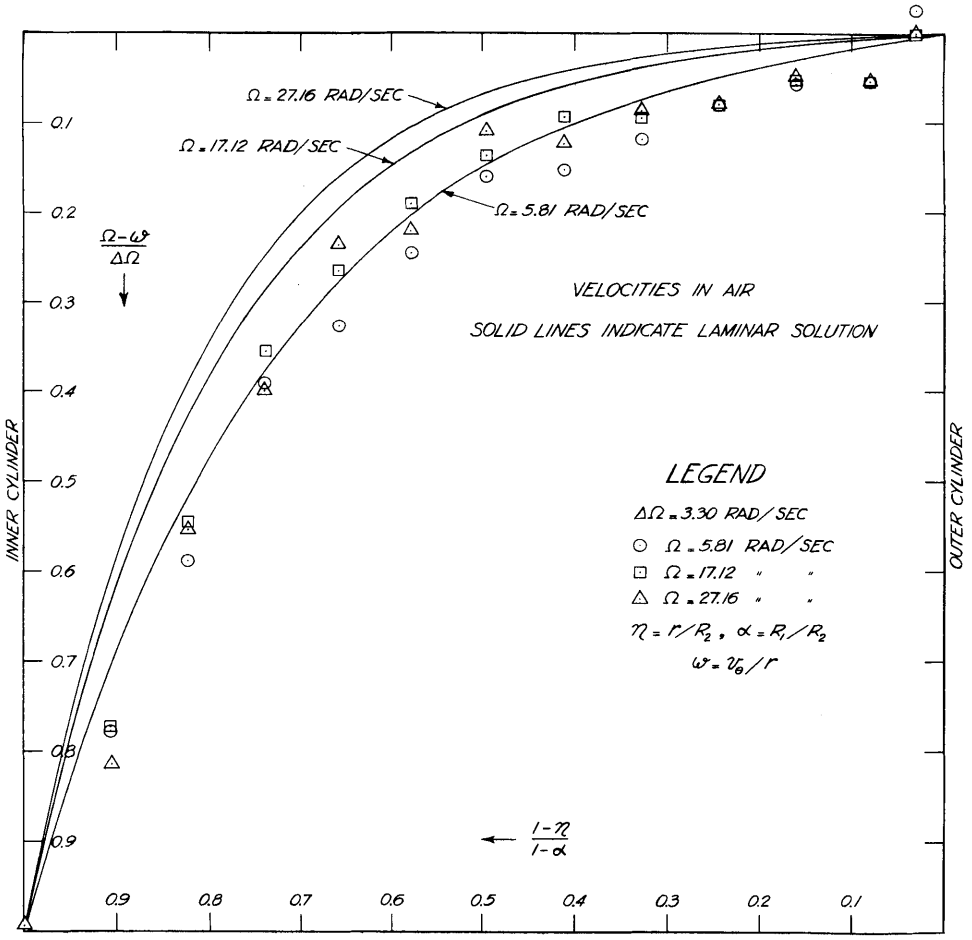

Tangential velocities in air

Figure 14

Velocities in air are presented in Figure 14. It is observed that both predicted curves and experimental data deviate further from the state of solid body rotation than do the curves and experimental data for similar conditions in water. This is due to the higher kinematic viscosity of air. The experimental data are for a constant value of $\Delta\Omega$ = 3.30 rad/sec, so that ε varies inversely as Ω. Although the value of ε, for Ω = 5.81 rad/sec, approaches a value of 0.6 the theory still appears to be in reasonable agreement with the data. The small amount of scatter in the air data is evidence that the measurements with the hot wire anemometer are more precise at high rates of rotating than the measurements with the impact tube-rotating manometer device.

A second set of velocity profiles in air, with a constant value of $\Delta\Omega$ = 6.60 rad/sec, is shown in Figure 15. The agreement between theory and experiment is remarkable, and is even better than for the case when $\Delta\Omega$ = 3.30 rad/sec. The reason for this is not well understood since intuitively one would expect increased turbulence at higher Reynolds numbers, and thus departure from the laminar theory.

In all experimental runs with air the output from the hot wire anemometer was displayed on an oscilloscope, and although it was difficult to visually detect differences in turbulence intensities, there is no doubt that the motion was turbulent for all runs. The turbulence intensities were calculated from measured rms voltages; they are shown in Figures 16 and 17. The turbulence intensity in Figure 16 is normalized by a constant velocity, $R\Delta\Omega$, whereas in Figure 17 the local mean tangential velocity relative to the probe is the normalizing factor. Both figures shown that the turbulence level is largest near the inner cylinder and decreases to a minimum near the outer cylinder. This

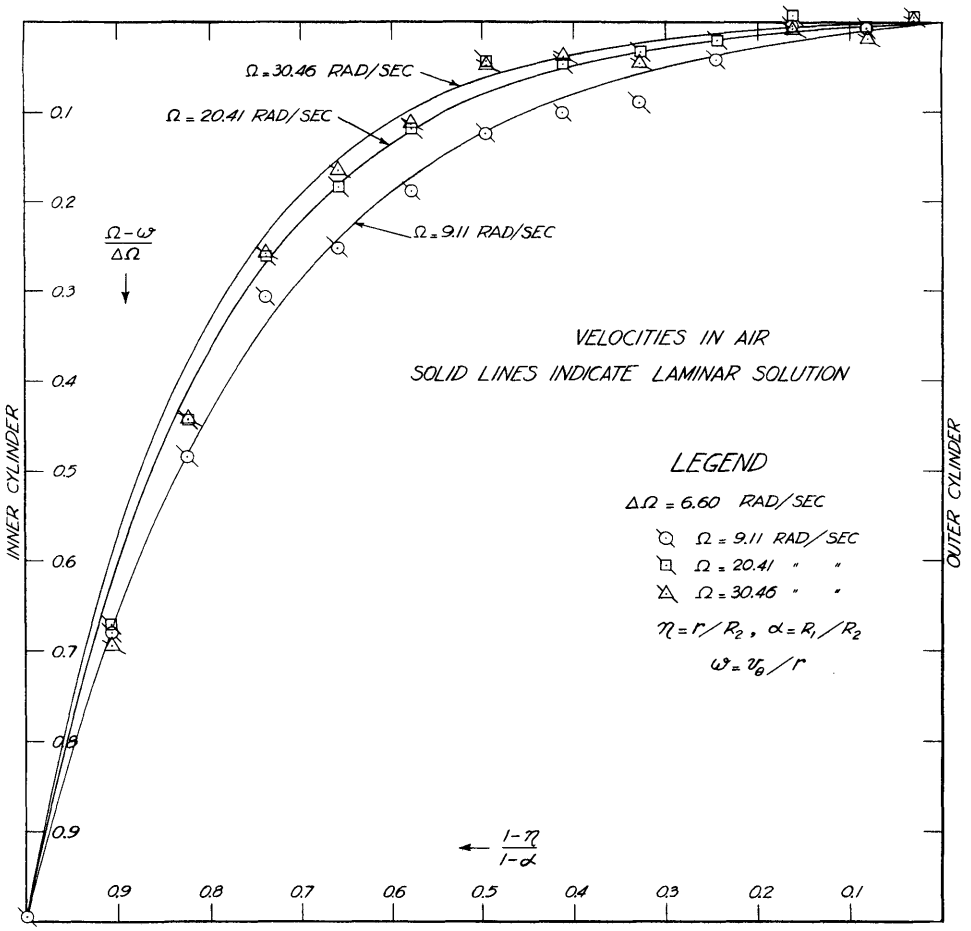

Tangential velocities in air

Figure 15

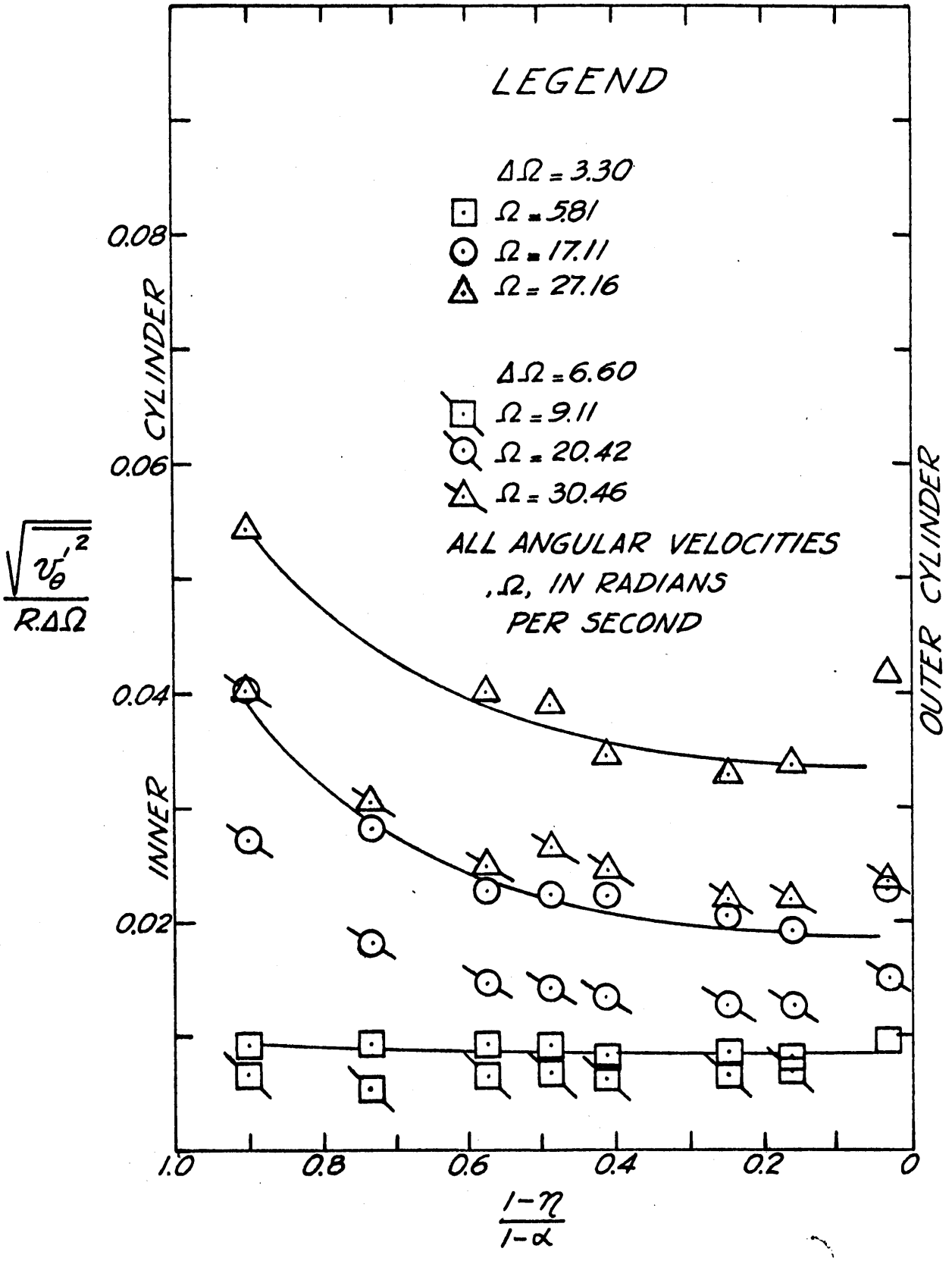

Turbulence intensities in air

Figure 16

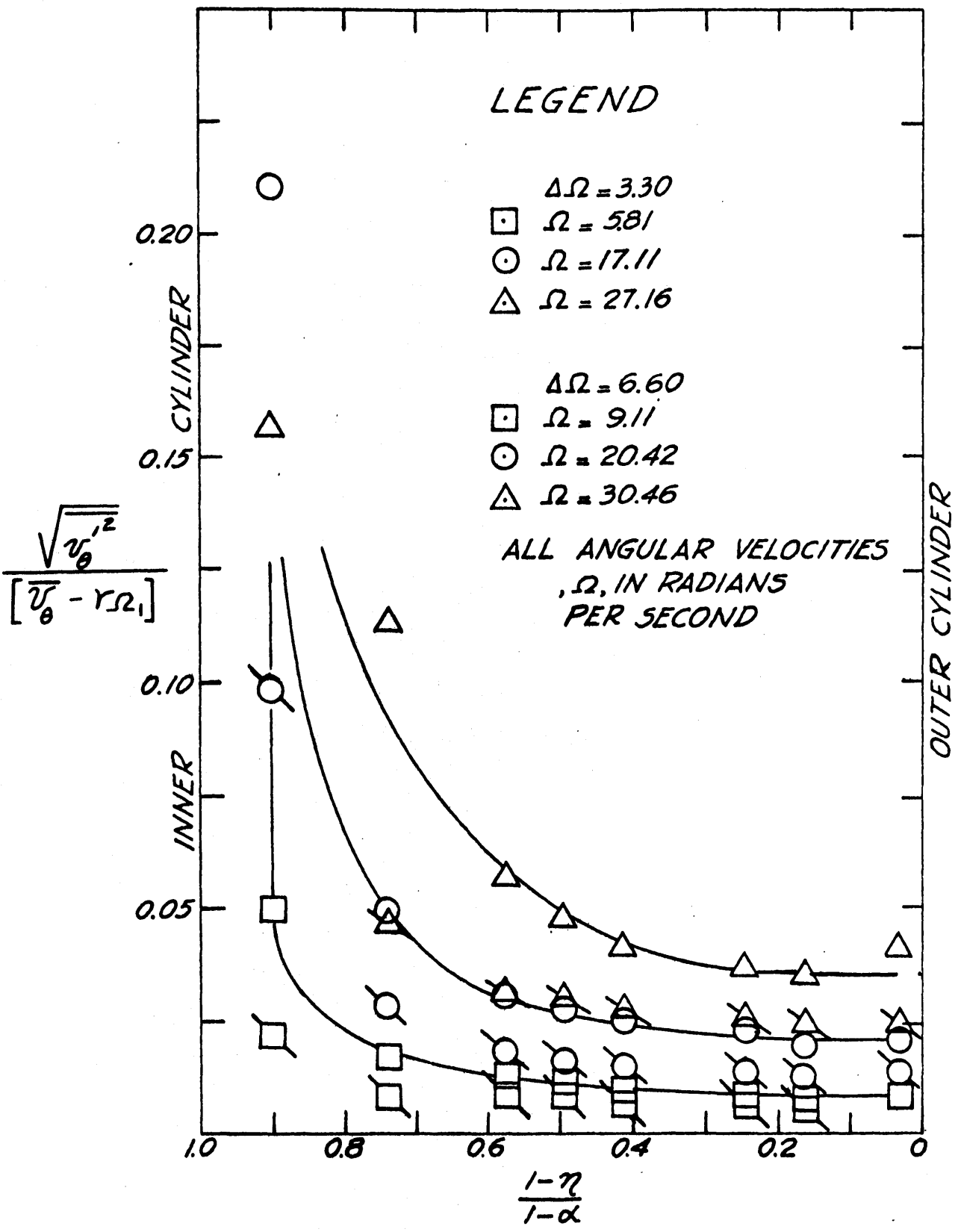

Turbulence intensities in air

Figure 17

trend is in agreement with the observed velocity distributions in the annular space which show an absence of shear at the outer cylinder wall. Observed turbulence intensities near the wall in pipe flow (18) are of the same order as those observed near the inner cylinder wall in the annulus.

An unexpected result is the fact that the turbulence intensities decrease when $\Delta\Omega$, or equivalently the Reynolds number, is increased. This appears to make plausible the fact that better agreement between theory and experiment in air was found when $\Delta\Omega = 6.60$ rad/sec as compared to $\Delta\Omega = 3.30$ rad/sec. However, the velocities in water showed the opposite trend, namely that an increase in $\Delta\Omega$ caused the experimental velocities to deviate further from the predicted ones. The trend that the turbulence intensities are increased for an increase in Ω, when $\Delta\Omega$ is kept constant, is perhaps due to imperfections in the apparatus. The intensity of vibrations for example are expected to grow with the rate of rotation.

Initial observations with a X-array hot wire probe at vertical locations other than mid-height have shown measurable changes in the direction of flow with changes in radial position in the annulus. Although these measurements are of a preliminary nature, they indicate that observations of secondary motion are feasible with the present equipment. A program involving detailed observation of secondary motion and comparison with the theory presented in Chapter 2 is planned.

CHAPTER V

CONCLUSIONS

In an attempt to explain the mechanism producing the unusual flow in the annular space between two concentric rotating cylinders of finite length, a solution for laminar flow conditions was developed. The solution was based on a linearization of the equations of motion using the ratio of the differential angular velocity to the angular velocity of the outer cylinder as a perturbation parameter, ε. It was found that the theory not only predicts the general nature of the velocity profiles but also is in reasonable agreement with detailed observation of the mean velocity profiles.

Mean velocity profiles observed at mid-height in the annular space in both water and air served to confirm the predictions from the theory. The theory predicts, and differentiates between, the velocity profiles in these two fluids having different viscosities. The experimental results in air were found to agree with the theory over a wider range of ε values than do the results in water.

In all of the experiments in air, the flow was observed to be turbulent, which makes the agreement between theory and experiment somewhat surprising. All measurements in air showed a decrease in the turbulence intensities with an increase in the differential angular velocity.

Recommendations for Future Work

In light of the above conclusions, a program of continuing investigations is recommended including:

1) Measurements of velocity, turbulence, and secondary motion at positions other than at mid-height. The instrumentation for these measurements has been developed.

2) A systematic study of the influence of the perturbation parameter, ε, and the Reynolds number on the characteristics of the flow.

3) Theoretical analysis of the boundary layer flow near the inner cylinder.

REFERENCES

1. Rayleigh, Lord. "On the Dynamics of Revolving Fluids," Proc., Roy. Soc., A, 1916, pp. 148 - 154.

2. Taylor, G. I. "Stability of a Viscous Liquid Contained Between Two Rotating Cylinders," Phil. Trans., A, Vol. 223, 1923, p. 289.

3. Taylor, G. I. "Distribution of Velocity and Temperature Between Concentric Cylinders," Proc., Roy. Soc., A, Vol. 151, 1935, p. 494.

4. Taylor, G. I. "Fluid Friction Between Rotating Cylinders," Parts I and II, Proc., Roy. Soc., A, Vol. 157, 1936, pp. 546 - 564.

5. Pai, S. "Turbulent Flow Between Rotating Cylinders," N.A.C.A. TN892, 1943.

6. Wendt, F. "Turbulente Strömungen Zwischen Zwei Rotierenden Koaxialen Cylindern," Ing. - Archiv., Band IV, Heft 6, September, 1933,

7. Coles, D. "Transition in Circular Couette Flow," J. Fluid Mech., Vol. 21, Part 3, 1965, pp. 385 - 425.

8. Greenspan, H. P. "On the General Theory of Contained Rotating Fluid Motions," J. Fluid Mech., Vol. 22, Part 3, 1965, pp. 449 - 462.

9. Wedemeyer, E. H. "The Unsteady Flow Within a Spinning Cylinder," J. Fluid Mech., Vol. 20, Part 3, 1964, pp. 383 - 399.

10. Ekman, W. "On the Influence of the Earth's Rotation on Ocean Currents," Arkiv. Mat. Astron. Fysik., Stockholm, Vol. 2 Nos. 1-2, 1905.

11. Prandtl, L. Essentials of Fluid Dynamics. Blackie & Son, Translated from the third edition, 1963.

12. Drinker, P. A., Gelhar, L. W., and W. Schriek. "The Development of a Rotating Endless Channel for Hydraulic and Sedimentary Studies," Hydrodynamics Laboratory Report No. 83, Department of Civil Engineering, M.I.T., September, 1965.

13. Runstadler, P. W., Kline, S. J., and W. C. Reynolds. "An Experimental Investigation of the Flow Structure of the Turbulent Boundary Layer," Report MD-8, Thermo Sciences Division, Department of Mech. Engr., Stanford University, Stanford, California, June, 1963.

14. Delleur, J. W. "Flow Direction Measurement with Hot Wire Anemometers," Presented at the Hydraulics Division Conference, Tucson, Arizona, August 25, 1965.

15. Greenspan, H. P. and L. N. Howard. "On a Time-Dependent Motion of a Rotating Fluid," J. Fluid Mech., Vol. 17, 1963, p. 385.

16. Roshko, A. "On the Development of Turbulent Wakes from Vortex Streets," Report 1191, N.A.C.A., 1954.

17. Rouse, H. Elementary Mechanics of Fluids, Wiley, 1946.

18. Hinze, J. O. Turbulence, McGraw-Hill, 1959.

APPENDIX A

LIST OF SYMBOLS

$B = (kE)^{1/2}$

c_1, c_2 constants

d shedding rod diameter

$E = R^2\Omega/\nu$ dimensionless number characterizing the Ekman layer

f vortex shedding frequency

h axial (vertical) scale of the motion

H vertical distance from mid-height to end plate in annulus

I heating current to hot wire anemometer

I_o heating current to hot wire anemometer at zero flow velocity

I_1 modified Bessel function

K_1 modified Bessel function

$k = (\nu/H^2\Omega)^{1/2}$

p pressure

q discharge per foot width

r radius

R_1 inner cylinder radius

$R_2 = R$ outer cylinder radius

Re Reynolds number

$S = fd/U$ Strouhal number

t width of annular space

U velocity

u dimensionless radial velocity component

v dimensionless tangential velocity component

w dimensionless axial velocity component

v_r radial velocity component

v_θ tangential velocity component

v_z axial velocity component

z axial co-ordinate

α ratio of inner cylinder radius to outer cylinder radius

η dimensionless radius

ξ dimensionless axial co-ordinate

$\varepsilon = \Delta\Omega/\Omega$ perturbation parameter

ρ density of fluid

μ dynamic viscosity of fluid

ν kinematic viscosity of fluid

ν_t eddy viscosity

ω angular velocity

Ω angular velocity of outer cylinder

Ω_1 angular velocity of inner cylinder

$\Delta\Omega$ differential angular velocity between cylinders

ψ dimensionless Stokes' stream function

APPENDIX B

The hot wire anemometer is used frequently in mean velocity and turbulence measurements in air. The air velocities are observed by measuring the rate at which heat is convected away from an electrically heated wire in the air stream. The theory of such measurements is discussed in detail by Hinze (18). In this study a constant temperature bridge-amplifier circuit was used, which maintains the temperature of the hot wire at a constant value, and the heat transfer from the wire is determined by measuring the power required to maintain this constant temperature. In a given Reynolds number range, based on the diameter of the hot wire, the electrical current, I, required to maintain a constant overheat temperature in the wire is linearly related to the square root of the flow velocity, U, past the wire (18), when the flow is perpendicular to the wire:

$$I^2 = A + B\sqrt{U} \qquad (1)$$

where A and B are constants depending on wire characteristics, overheat ratio in the wire and fluid properties of the flow. The constants A and B are evaluated from a calibration of I^2 versus $\sqrt{U}$.

Experiments (14) have indicated that when the length-diameter ratio of the hot wire exceeds one hundred, and when the angle between the flow direction and the wire is larger than 20°, there is no coupling between the temperature in the wire and the axial velocity component past the wire. In applications where the direction of flow is not perpendicular to the wire, the axial velocity component may therefore by neglected as long as the intersection angle between wire and velocity vector is larger than 20°. Equation 1 then can be written:

$$I^2 = A + B\sqrt{U \sin \gamma} \qquad (2)$$

where γ is the angle between hot wire and velocity vector. The power is thus seen to be dependent on the angle γ. When velocity fluctuations are introduced, only those in a plane perpendicular to the wire need be considered and the instantaneous velocity normal to the wire is

$$U = [(\bar{u} + u')^2 + v'^2]^{1/2}$$

where $\bar{u}$ is the mean velocity

u' is the velocity fluctuation in the direction of $\bar{u}$

v' is the velocity fluctuation normal to $\bar{u}$.

The fluctuations in the flow require fluctuations in the energy supplied to the wire, which can be written in terms of current fluctuations:

$$I = \bar{i} + i'$$

By introducing these variables into equation 1 and including only terms of first order in fluctuating quantities the following linearized relationships can be derived (18).

$$\bar{i}^2 = A + B\sqrt{\bar{u}} \qquad (3)$$

$$i' = \frac{B\sqrt{\bar{u}}}{4\bar{i}} \cdot \frac{u'}{\bar{u}} \qquad (4)$$

When the flow velocity $\bar{u}$ is zero, the required heating current is defined as I_o so that equation 3 can be written:

$$\frac{\bar{i}^2 - I_o^2}{I_o^2} = \frac{B}{I_o^2}\sqrt{\bar{u}} \qquad (5)$$

Typical calibration curves of this form are shown in Figure 18.

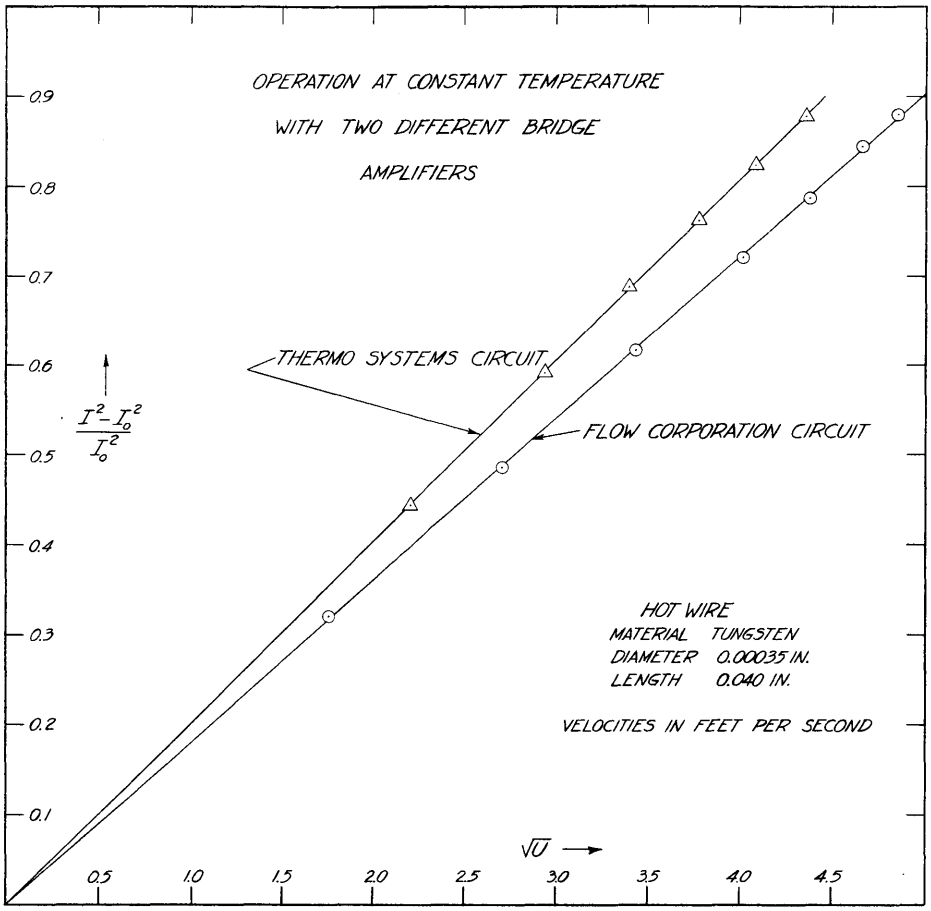

Typical hot-wire anemometer calibration curves

Figure 18

Taking the root mean square of equation 4 yields:

$$\sqrt{\frac{\overline{u'^2}}{\bar{u}}} = \frac{4\bar{i}}{B\sqrt{\bar{u}}}\sqrt{\overline{i'^2}} \tag{6}$$

Equations 5 and 6 were used throughout for the calculations of mean velocities and turbulent fluctuations respectively.

To obtain an estimate of the neglected second order or higher order terms it is necessary to include these terms in the equations. The time average of the equation, including second order terms only, is (18):

$$(\bar{i}^2 + \overline{i'^2}) = I_o^2 + B\sqrt{\bar{u}}\left[1 - \frac{1}{8}\frac{\overline{u'^2}}{\bar{u}^2} + \frac{1}{4}\frac{\overline{v'^2}}{\bar{u}^2}\right] \tag{7}$$

The size of the term $\overline{i'^2}$ on the left hand side of equation 7 may be estimated from equation 4. Equation 7 may then be written:

$$\bar{i}^2 = I_o^2 + B\sqrt{\bar{u}}\left(1 - \frac{1}{8}\frac{\overline{u'^2}}{u'^2} + \frac{1}{4}\frac{\overline{v'^2}}{\bar{u}^2} - \frac{1}{16}\frac{B\sqrt{\bar{u}}}{\bar{i}^2}\frac{\overline{u'^2}}{\bar{u}^2}\right) \tag{8}$$

The quantity $B\sqrt{\bar{u}} / \bar{i}^2$ is seen from equation 5 to be at most of order 1. For the work reported herein the maximum observed turbulence intensity, $\left(\frac{\overline{u'^2}}{\bar{u}}\right)^{1/2}$, at the inner cylinder wall is of the order of 25 per cent. This measurement is itself a result of a linearization, but is adequate for a first estimate of the influence of the second order terms on the value of $\bar{u}$. The turbulence intensities in the radial direction are expected to be smaller than those in the tangential direction by an analogy to pipe flow, for instance (18). A reasonable approximation

for $(\overline{v'^2})^{1/2} / \bar{u}$ is one half of the value of $(\overline{u'^2})^{1/2} / \bar{u}$, in which case the term in brackets on the right hand side of equation 8 differs from unity by 0.78 per cent. Therefore equation 5 may be used to determine the mean velocity $\bar{u}$ with a maximum error of 1.6% due to second order effects.

```
C     COMPUTER PROGRAM FOR CALIBRATION OF HOT WIRE ANEMOMETER
C     PROGRAMMED IN FORTRAN 2 ON IBM 1620 COMPUTER
*     ID  SCHRIEK, W.        4527      CALIBRATION
*     SUBSET
C     CALIBRATION OF 0.00035 INCH DIAMETER HOT WIRE
C     USING FLOW CORP. ANEMOMETER
C     INITILIZE VARIABLES FOR LEAST SQUARES PROCEDURE
C     X IS NORMALIZED CURRENT QUANTITY
C     Y IS SQUARE ROOT OF VELOCITY
      NO=0
      SUMX=0
      SUMY=0
      SUMXY=0
      SUMX2=0
C     TEMP=AIR TEMPERATURE ON DAY OF CALIBRATION (DEGREES F)
      READ 100, TEMP
C     VISC OF AIR IS EXPRESSED AS A FUNCTION OF TEMPERATURE
      VISC=1.58E-04+(TEMP-60.)*5.5E-07
      PUNCH 108, TEMP, VISC
C     N=NUMBER OF SHEDDING RODS USED
      READ 101, N
      PUNCH 104
      DO 1 M=1,N
C     SPECIFY ROD DIAMETER, SPECIFY AREA CORRECTION COEFFICIENT (COE)
      READ 102, DIAM, COE
C     L=NUMBER OF CALIBRATION PTS FOR EACH DIAMETER, AMPO=ZERO FLOW CURRENT
      READ 103, L, AMPO
      DO 1 J=1,L
C     FREQ IS OBSERVED FREQUENCY OF VORTEX SHEDDING
C     AMP IS OBSERVED CURRENT FROM BRIDGE AMPLIFIER
      READ 105, FREQ, AMP
      A=(FREQ*DIAM)/(0.212*12.)
      B=(21.2*VISC*12.)/DIAM
      C=(12.7*VISC*12.)/DIAM
      AMP2=AMP**2
      AMPO2=AMPO**2
      AMPA=(AMP2/AMPO2-1.)
C     TRIAL AND ERROR SOLUTION FOR VELOCITY FROM STROUHAL-REYNOLDS RELATION
C     VEL IS THE AVERAGE VELOCITY OF AIR STREAM PAST HOT WIRE
      VEL=A+B
      RE=(VEL*DIAM)/(VISC*12.)
      IF(150.-RE) 3,3,12
    3 IF(RE-300.) 5,5,4
    4  VEL=A+C
      RE=(VEL*DIAM)/(VISC*12.)
      IF(RE-300.) 5,5,12
    5  IF(.091-DIAM) 6,7,8
    6 DO 9 K=1,2
      VEL=A+0.207+0.00093*(300.-RE)
    9 RE=(VEL*DIAM)/(VISC*12.)
      GO TO 12
    7 DO 10 K=1,2
      VEL=A+0.285+0.00127*(300.-RE)
   10 RE=(VEL*DIAM)/(VISC*12.)
      GO TO 12
    8 DO 11 K=1,2
      VEL=A+0.405+0.0018*(300.-RE)
   11 RE=(VEL*DIAM)/(VISC*12.)
   12 VEL=COE*VEL
      VEL5=SQRT(VEL)
      PUNCH 106,VEL,VEL5,AMPA,RE
      X=AMPA
      Y=VEL5
      SUMX=SUMX+X
      SUMY=SUMY+Y
      SUMXY=SUMXY+X*Y
      SXSY=SUMX*SUMY
      SUMX2=SUMX2+X**2
    1 NO=NO+1
      P=NO
C     U IS THE INTERCEPT ON SQUARE ROOT OF VELOCITY AXIS
C     V IS THE SLOPE OF SQUARE ROOT OF VELOCITY VS CURRENT QUANTITY PLOT
      U=(SUMY*SUMX2-SUMXY*SUMX)/(P*SUMX2-SUMX**2)
      V=(SXSY-P*SUMXY)/(SUMX**2-P*SUMX2)
      PUNCH 107, U, V
  100 FORMAT (F10.3)
  101 FORMAT (I1)
  102 FORMAT (2F10.4)
  103 FORMAT (I10, F10.3)
  104 FORMAT (5X,4H VEL,5X,5H VEL5,7X,5H AMPA,10X,3H RE /)
  105 FORMAT (F10.5, F10.5)
  106 FORMAT (4X,F7.3,4X,F6.3,5X,F6.3,7X,F7.0)
  107 FORMAT (// 8X,21H LEAST SQUARE LINE IS / 14X,3H Y=,F8.4,2H +,F8.4,
     12H X)
  108 FORMAT (//6H TEMP=,F6.2,5X,6H VISC=,E10.3 //)
      END
```

```
C     COMPUTER PROGRAM FOR CALCULATION OF MEAN VELOCITIES + TURB. INTENSITIES
C     PROGRAMMED IN FORTRAN 2 ON IBM 1620 COMPUTER
*     ID  SCHRIEK, W.        4527      RUN
*     SUBSET
C     N=NUMBER OF DIFFERENT DISTANCES IN TRAVERSE
C     S=SLOPE OF NORMALIZED CALIBRATION CURVE
C     DISTO=LENGTH OF PROBE INSIDE APPARATUS WHEN WIRE IS AT INNER CYLINDER
      READ 108, N, S,DISTO
      PUNCH 111
      DO 1 I=1,N
C     DIST1=MEASURED DISTANCE
C     AMPO=ZERO FLOW CURRENT
      READ 109,DIST1,AMPO
      DIST=15.+DISTO-DIST1
      DO 1 J=1,6
C     REV1 AND REV2 ARE INNER AND OUTER CYL SPEEDS AS MEASURED
C     AMP=CURRENT READINGS
C     RMS IS THE ROOT MEAN SQUARE VALUE OF CURRENT USED IN TURB. CALCULATIONS
      READ 109, REV1,REV2,AMP,RMS
      A2=AMP**2
      AO2=AMPO**2
      Y=(A2-AO2)/AO2
      X=0.1034+2.9353*Y
      VEL5=X
      VEL=(VEL5**2)
      B=4.0/(1.0-AO2/A2)
C     TURBR=TURB. INTENSITY NORMALIZED BY LOCAL MEAN VELOCITY
      TURBR=RMS*B/AMP
      W1=(0.01256*REV1)
      W2=(0.01256*REV2)
      DW=W2-W1
C     VELI=VELOCITY OF INNER CYLINDER
      VELI=1.25*W1
C     VELO=VELOCITY OF OUTER CYLINDER
      VELO=1.502*W2
C     TURBA=TURB. INTENSITY NORMALIZED BY CONSTANT DIFFERENTIAL VELOCITY
      TURBA=(TURBR*VEL)/1.5*DW
C     VELA=ABSOLUTE VELOCITY
      VELA=VEL+(DIST*W1/12.)
    1 PUNCH 110,VELA,DIST,TURBR,TURBA,W1,W2,DW,VELI,VELO
  108 FORMAT (110,2F10.5)
  109 FORMAT (4F10.5)
  110 FORMAT(2(F7.3,2X),2(F8.4,2X),3(F6.2,2X),F7.3,2X,F7.3)
  111 FORMAT(//1X,5H VELA,5X,5H DIST,3X,6H TURBR,4X,6H TURBA,5X,3H W1,
     15X,3H W2,5X,3H DW,5X,5H VELI,4X,5H VELO /)
      END
```

```
C     COMPUTER PROGRAM FOR CALCULATION OF PREDICTED VELOCITIES AND COORDINATES
C     OF STREAMLINES IN ANNULAR SPACE
C     PROGRAMMED IN FORTRAN 2 ON IBM 1620 COMPUTER
*     ID SCHRIEK W.          E1673      DSR4527
*     SUBSET
C     LAMINAR SOLUTION FOR THE INTERIOR REGION
C     Z IS VERTICAL COORDINATE
      DIMENSION PSI (10), Z (10), VISCW (20)
C     A IS NONDIMENSIONAL INNER RADIUS
      READ 1,A
      SA=SQRT(A)
      ASA=A*SA
      DO 43 J=1,20
C     VISCW IS STORED ARRAY OF KINEMATIC VISCOSITIES OF WATER
   43 READ 15, VISCW(J)
      DO 2 K=1,10
C     PSI IS THE VALUE OF NONDIMENSIONAL STREAM FUNCTION
    2 READ 1,PSI(K)
C     TEMP IS AMBIENT AIR TEMPERATURE (DEGREES F)
C     FLUID=1.0 STANDS FOR WATER, FLUID=2.0 STANDS FOR AIR
      READ 40, TEMP, FLUID
      IF (1.0-FLUID) 41,42,19
   19 PUNCH 50
C     AIR VISCOSITY IS EXPRESSED AS FUNCTION OF TEMPERATURE
   41 VISC=1.25E-04 +5.5E-07*TEMP
      PUNCH 16
      GO TO 11
   42 DUM=TEMP-60.0
      J=DUM
C     WATER VISCOSITY OBTAINED FROM STORED ARRAY
      VISC=VISCW(J)
      PUNCH 17
C     OMA IS ANGULAR VELOCITY IN RADIANS PER SECOND
   11 READ 1,OMA
      PRINT 13,OMA
      PRINT 12
      B=1.5*(OMA**.25)/(VISC**.25)
      Q=.0065/(OMA**.5)
C     PSIM IS MAXIMUM VALUE OF THE STREAMFUNCTION
      PSIM=Q*(A**2)
      BATA=B*(1.0-A)
C     SINH BATA IS EXPRESSED AS A SERIES EXPANSION
      E=1.0
      N=1
      SINHA=BATA
    5 N=N+1
      K=(2*N)-1
      F=K
      E=E*F*(F-1.0)
      D=(BATA**K)/E
      SINHA=SINHA+D
      IF (D-.000114)4,4,5
C     TRAVERSE THE ANNULAR SPACE IN 1/4 INCH INCREMENTS
    4 DO 3 M=60,71
      N=M-59
      Y=M
C     R IS RADIUS IN FEET
      R=Y/48.0
C     ETA IS NONDIMENSIONAL RADIUS
C     IF ETA=1.0 DEFINE VERTICAL COORDINATE EQUAL TO 1.0
      ETA=R/1.502
      SETA=SQRT(ETA)
      BETA=B*(1.0-ETA)
      IF (BETA)20,20,21
C     SINH BETA IS EXPRESSED AS A SERIES EXPANSION
   21 E=1.0
      N=1
      SINHE=BETA
    7 N=N+1
      K=(2*N)-1
      F=K
      E=E*F*(F-1.0)
      C=(BETA**K)/E
      SINHE=SINHE+C
      IF (C-.0001)6,6,7
C     V IS THE TANGENTIAL VELOCITY
    6 V= (ASA*SINHE)/(SETA*SINHA)
C     ZETA = 1-ETA/1-ALPHA
      ZETA=BETA/BATA
      ZOMA=V/ETA
      PRINT 9,R,V,ETA,ZETA,ZOMA
      DO 30 I=1,10
      P=PSI(I)
      Z(I)= (P*SA*SINHA)/(SETA*SINHE)
      IF (Z(I)-999.0) 30,30,31
   31 Z(I)=999.0
   30 CONTINUE
      PRINT 10,(Z(I),I=1,10)
      GO TO 3
   20 ZZ=1.0
      PRINT 1,ZZ
    3 CONTINUE
    1 FORMAT (F10.5)
    9 FORMAT (/6F10.4)
   10 FORMAT (10F8.3)
   12 FORMAT (//49H PARAMETERS ARE PRINTED IN THE FOLLOWING SEQUENCE//49
     1H RADIUS     VELOCITY     ETA       ZETA       ZOMA/35H VERTICAL CO
     1ORDINATES FOR GIVEN ETA)
   13 FORMAT (/9H OMEGA ISF6.2,19H RADIANS PER SECOND)
   15 FORMAT (E10.3)
   16 FORMAT (//13H FLUID IS AIR //)
   17 FORMAT (//15H FLUID IS WATER //)
   40 FORMAT (2F10.5)
   50 FORMAT (24H ERROR IN DEFINING FLUID )
      GO TO 11
      END
```


APPENDIX C. Computer Programs